Tutorial Vol. 41, No. 4 / April 2024 / Journal of the Optical Society of America A 615

Journal of the Optical Society of America A

OPTICS, IMAGE SCIENCE, AND VISION

Nonstationary optics: tutorial

MATIAS KOIVUROVA,* JYRKI LAATIKAINEN, AND ARI T. FRIBERG

Center for Photonics Sciences, Department of Physics and Mathematics, University of Eastern Finland, P.O. Box 111, 80101 Joensuu, Finland
**matias.koivurova@uef.fi*

Received 2 January 2024; revised 18 February 2024; accepted 19 February 2024; posted 22 February 2024; published 11 March 2024

Over the past several decades, nonstationary optics has risen as a key enabling technology for a multitude of novel applications. These include areas of research such as micromachining and ultrafast optics, as well as the Nobel awarded research in femtochemistry, optical frequency combs, and attosecond physics. This tutorial aims to present some of the main concepts required to analyze nonstationary fields, with an emphasis on pulsed beams. The work begins from the fundamental building blocks of such fields, and builds up to some of their main properties. The spatiotemporal properties and stability of such fields are discussed in length, and some common measurement schemes are reviewed.

https://doi.org/10.1364/JOSAA.516951

1. INTRODUCTION

Nonstationary optics is a branch of photonics research, where the main focus is on transient phenomena in electromagnetic fields. In the broadest sense, this includes any type of time-dependent fluctuation of a fully three-dimensional field, be it in amplitude, phase, or polarization. In practice, however, it is usually desirable to restrict one's attention to a much narrower class of fields: pulsed beams. Although such fields present only a small subset of all possible nonstationary fields, they contain a multitude of properties not found in statistically stationary fields. In particular, pulses have a finite duration, which can be used to investigate processes on the same time scale. The pulse duration is also inversely related to the width of the pulse spectrum, so that a broader spectrum can support a shorter pulse. This in turn means that a pulsed laser comes with a nonzero frequency bandwidth. Moreover, pulses offer the possibility of achieving very high peak powers, with the current record being on the order of 10^{23} W/cm^2 [1].

It is the aim of the present work to underline some of the main properties of nonstationary fields, and to show how they are relevant in cutting-edge research performed today. Indeed, pulses are the modern workhorse for many advanced applications, such as micromachining [2–4], femtochemistry [5–7], optical frequency metrology [8–10], photonic and plasmonic Bose–Einstein condensation [11,12], as well as ultrafast spectroscopy [13], to name a few. The newest frontier in nonstationary optics is attosecond science [14,15], which employs optical pulses on the order of several tens to hundreds of attoseconds [16–18]. These can be used to directly measure the electric field of light [19] or observe electron dynamics [20–22] or the buildup of quantum interference [23,24]. The present tutorial is applicable to pulses of any duration and bandwidth, while the ideas, mathematical formulation, as well as measurement schemes can be extended to more general nonstationary fields.

The tutorial is structured as follows: we begin by giving definitions of the mathematical procedures and the desired fields in Section 2. In Section 3 we expand the discussion with the use of correlation functions, and show how statistically stationary fields can be viewed as a limiting case of nonstationary fields. Then we move on to the properties of nonstationary fields in Section 4, after which we introduce some instrumentation and measurement schemes in Sections 5 and 6, respectively. We then briefly mention some topics that fall outside the scope of the tutorial and give concluding remarks in Section 7.

2. ELECTROMAGNETIC FIELD

We begin by defining the types of waves we are interested in. Light is an electromagnetic wave, although usually it is enough to consider only the electric field, since most materials are nonmagnetic at optical frequencies. Let us say that we have a dielectric with a refractive index n, which is homogeneous and isotropic, so that n does not depend on position or polarization. To account for dispersion, we employ the Helmholtz equation

$$\nabla^2 \tilde{\boldsymbol{E}}(\mathbf{r};\omega) = -k^2(\omega)\,\tilde{\boldsymbol{E}}(\mathbf{r};\omega), \tag{1}$$

where $k(\omega) = k_0 n(\omega)$ with $k_0 = 2\pi/\lambda_0$ being the vacuum wave number with the corresponding vacuum wavelength λ_0. Equivalently, we can write $k(\omega) = \omega/c(\omega)$, where $\omega = 2\pi c_0/\lambda_0$ is the frequency, and $c(\omega) = c_0/n(\omega)$ is the phase speed of the wave, with c_0 being the speed of light in vacuum. In Euclidean space, the general electric field vector that satisfies the Helmholtz equation has three scalar components:

$$\tilde{\boldsymbol{E}}(\mathbf{r};\omega) = \begin{bmatrix} \tilde{E}_x(\mathbf{r};\omega) \\ \tilde{E}_y(\mathbf{r};\omega) \\ \tilde{E}_z(\mathbf{r};\omega) \end{bmatrix}, \tag{2}$$

where the subscripts denote the three possible spatial directions and the position vector contains the Cartesian coordinates $\mathbf{r} = (x, y, z)$. We choose that the wave propagates towards the positive half space $z > 0$. For now, we are going to restrict our attention to single scalar components, which can be either the x or y polarization in the present basis. It is also possible to consider a different basis where the left and right circular polarizations are the relevant scalar components.

Although the electromagnetic field is real valued, we often use the complex analytic signal (see, e.g., [25], p. 92 *et seq.*), since it is mathematically convenient. The complex analytic signal allows us to write Fourier transform pairs of the form

$$E(\mathbf{r};t) = \int_0^\infty \tilde{E}(\mathbf{r};\omega)\exp(-i\omega t)\mathrm{d}\omega, \tag{3}$$

$$\tilde{E}(\mathbf{r};\omega) = \frac{1}{2\pi}\int_{-\infty}^\infty E(\mathbf{r};t)\exp(i\omega t)\mathrm{d}t, \tag{4}$$

where t is time, and the lower bound of zero in the frequency integral is due to analyticity. Note that we denote frequency domain fields with a tilde. This particular Fourier pair describes how components with different frequencies, ω, have to be distributed to get the temporal field $E(\mathbf{r};t)$. Moreover, the real field is retrieved with

$$E^{(\mathrm{re})}(\mathbf{r};t) = \Re\{E(\mathbf{r};t)\}, \tag{5}$$

where $\Re$ stands for the real part.

The simplest solution to the Helmholtz equation is a homogeneous monochromatic plane wave

$$E(\mathbf{r};t) = \sqrt{I}\exp(i\boldsymbol{k}\cdot\mathbf{r} - i\omega_c t + i\phi_0), \tag{6}$$

given here in the time domain. Here $\sqrt{I}$ is the amplitude of the wave, $\boldsymbol{k} = (k_x, k_y, k_z)$ is the wave vector, with the magnitude $|\boldsymbol{k}| = k = k_0 n(\omega_c)$, ω_c is the carrier frequency, and ϕ_0 is an arbitrary phase factor. This solution is perfectly stationary, since all of its statistical moments are constant (see [25], p. 11 *et seq.*). Most notably, the second moment, which we call average intensity, is simply $\langle|E(\mathbf{r};t)|^2\rangle = I$, where angle brackets denote averaging. We will discuss the possible averaging methods in detail in the beginning of Section 3.

Armed with the simplest possible solution to the Helmholtz equation, we can now draft what a nonstationary field looks like. Although a single plane wave is stationary, we can use a superposition of two (or more) plane waves to obtain a nonstationary solution. This is mathematically possible, since the Helmholtz equation is linear. That is, all linear combinations of solutions are also solutions. Therefore, we take two fields $E_1(t) = 1/2\exp(-i\omega_1 t)$ and $E_2(t) = 1/2\exp(-i\omega_2 t)$, with the frequencies ω_1 and ω_2, respectively, and let them interfere,

$$\begin{aligned} E_1(t) + E_2(t) &= \frac{1}{2}\exp(-i\omega_1 t) + \frac{1}{2}\exp(-i\omega_2 t), \\ &= \frac{1}{2}\exp(-i\omega t)\left[\exp(-i\Delta\omega t/2) + \exp(i\Delta\omega t/2)\right], \\ &= \exp(-i\omega t)\cos(\Delta\omega t/2), \end{aligned} \tag{7}$$

where $\Delta\omega = \omega_2 - \omega_1$ is the difference frequency, $\omega = (\omega_1 + \omega_2)/2$ is the mean frequency, and we have left space dependence implicit. We use the symbol ω for the mean frequency, although it was used as the symbol for the absolute frequency above. The reasoning behind this choice will become apparent in Section 3.A. From here we immediately see that intensity is given by $I(t) = |E_1(t) + E_2(t)|^2 = \cos^2(\Delta\omega t)$. Hence, the superposition of two statistically stationary (and mutually correlated) fields of different frequencies yields a nonstationary field. From this statement it follows that a pulse cannot be stationary since it will contain more than one frequency, which are correlated. This is the basis on which we shall build the rest of the tutorial (in a similar fashion as in [26]).

3. CORRELATION FUNCTIONS

To move forward, we will need a short survey on partial coherence. What sets partially coherent light apart from coherent light is that the plane wave components that make up the field might not be completely *correlated* with each other. Wolf adapted the ideas of Zernike [27], and defined spatial coherence as the ability of two fields to produce visible, time-averaged, spatial interference fringes in an interferometric measurement ([25], p. 151). This is one possible definition (and probably the most common one), although it is not the only possibility. The motivation behind this definition is to tie correlation explicitly to experiments, where we always use slow, time-averaging detectors to observe the interference. Since time-averaging detectors will also average over temporal interference fringes, such measurements do not allow for the study of spectral and temporal correlations.

If we take the superposition of two plane waves as a concrete example, we know that (i) the two waves are individually completely coherent and (ii) they have a constant, well-defined phase relation between each other. Thus, one would expect that the resulting superposition is also completely coherent. However, taking the time average over the interference pattern we find that

$$\lim_{T\to\infty}\frac{1}{T}\int_0^T \cos^2(\Delta\omega t/2)\,\mathrm{d}t = 1/2, \tag{8}$$

which means that the interference pattern is not visible with slow detectors, and one might conclude that the two plane wave components are not correlated. If we instead suppose that the frequency difference between the plane waves is very small, such that $1/\Delta\omega$ is much greater than the exposure time of the detector, we will see a slowly modulated intensity at the detector, i.e., a temporal interference pattern. Now, if the two plane wave components have a randomly varying phase difference, the intensity fluctuations will again wash out. Therefore, we can conclude that for nonstationary fields it is more appropriate to look at the phase relation between the frequency components instead. The experimental aspects related to this are examined in more detail in Section 6.A.

Examples of partial coherence can be found everywhere: blackbody radiation, LEDs, multimode lasers, free-electron lasers, synchrotron x-ray sources, etc. In fact, all real light sources are partially coherent. Some, such as single mode lasers, are very coherent, while others, such as incandescent light bulbs, are very incoherent. But there are no sources that are completely coherent (or incoherent), only those that are very close to the ideal

situations. Coherence research usually begins by supposing that the electromagnetic field is a random process. Thus, expected values are of interest, so we take averages over an ensemble of individual *realizations*. Realizations may be single pulses picked from a long train of pulses, or long time sections taken from a continuous wave source. If the members of the ensemble are denoted with $f_n(t)$, then the ensemble average is defined as

$$\langle f(t)\rangle = \lim_{N\to\infty} \frac{1}{N}\sum_{n=1}^{N} f_n(t). \tag{9}$$

Note that by using the ensemble average, we can circumvent the problems of using the time average with nonstationary fields. Employing the ensemble average, we will next define the correlation functions in the various domains of interest.

A. Spectral Coherence

For simplicity, we will continue to ignore the spatial dependence of the field in the next few subsections. In general, the spectral field $\tilde{E}(\omega)$ varies from pulse to pulse. We say that it is a random process, where each spectral point characterized by ω is a random variable. This way, we can come up with a quantitative measure for most amplitude or phase fluctuations, which is the two-frequency cross-spectral density function (CSD), defined as

$$W(\omega_1,\omega_2) = \langle \tilde{E}^*(\omega_1)\tilde{E}(\omega_2)\rangle, \tag{10}$$

where the asterisk denotes complex conjugate. This is essentially the expected value of the product between the random variables $\tilde{E}(\omega_1)$ and $\tilde{E}(\omega_2)$. That is, the CSD compares the field to itself at frequencies ω_1 and ω_2. We can find the *energy spectrum* (also known as the spectral energy density) by setting $\omega_1 = \omega_2 = \omega$,

$$S(\omega) = W(\omega,\omega) = \langle |\tilde{E}(\omega)|^2\rangle. \tag{11}$$

The above expression should not be confused with the power spectrum found in stationary theory. Simple dimensional analysis shows that the above quantity describes how energy is spread across different frequencies [28], which can also be deduced from Parseval's theorem. This quantity is the main definition of spectrum from the theoretical point of view [29–32], whereas the so-called time-dependent physical spectrum can be experimentally relevant (see [33] for more information).

Here, we will briefly comment on the usage of the symbol ω as the mean frequency. It is possible to introduce a coordinate rotation, such that we move from the absolute coordinates (ω_1,ω_2) to the average and difference coordinates $(\omega,\Delta\omega)$. Under this rotation, the CSD is $W(\omega,\Delta\omega)$, in which case the spectral density is given by $S(\omega) = W(\omega,0)$, since $\Delta\omega = \omega_2 - \omega_1$. Therefore, the mean frequency is representative of the absolute frequency of the spectral density one would measure, for any state of coherence.

We can use the energy spectrum to define the complex degree of spectral coherence, by normalizing the CSD with the corresponding energy spectra, as in

$$\mu(\omega_1,\omega_2) = \frac{W(\omega_1,\omega_2)}{\sqrt{S(\omega_1)S(\omega_2)}}. \tag{12}$$

The complex degree of coherence satisfies the inequalities

$$0 \le |\mu(\omega_1,\omega_2)| \le 1, \tag{13}$$

where the minimum and maximum correspond to no correlation and complete correlation in the field, respectively, between frequencies ω_1 and ω_2.

If all of the field realizations are identical, then every member of the ensemble has the same form as the average. Therefore, we can write [34]

$$W(\omega_1,\omega_2) = \mathcal{E}^*(\omega_1)\mathcal{E}(\omega_2). \tag{14}$$

Substituting this into Eq. (12), we immediately see that $|\mu(\omega_1,\omega_2)| = 1$ for all ω_1 and ω_2. Thus, the field is completely coherent, which is equivalent to having a correlation function that factors into ω_1 and ω_2 dependent parts.

Last, we can define an *overall degree of spectral coherence*, as in

$$\bar{\mu} = \sqrt{\frac{\int_0^\infty\int_0^\infty |W(\omega_1,\omega_2)|^2 \mathrm{d}\omega_1\mathrm{d}\omega_2}{\int_0^\infty\int_0^\infty S(\omega_1)S(\omega_2)\mathrm{d}\omega_1\mathrm{d}\omega_2}}, \tag{15}$$

which is essentially a root-mean-squared average over the degree of coherence. The overall degree of coherence is also limited to the interval [0, 1], again signifying complete incoherence and coherence, respectively. Note that this does not depend on the frequency coordinates, and it is instead an average measure of coherence over the whole field.

B. Temporal Coherence

We can proceed in the time domain in a similar fashion, and define the mutual coherence function (MCF) as

$$\Gamma(t_1,t_2) = \langle E^*(t_1)E(t_2)\rangle. \tag{16}$$

This is again a measure of correlations in the field between two instants of time t_1 and t_2. We can use Eq. (3) to form a relation between the MCF and the CSD; this is can be viewed as a generalized Wiener–Khintchine theorem,

$$\Gamma(t_1,t_2) = \iint_0^\infty W(\omega_1,\omega_2)\exp[i(\omega_1 t_1 - \omega_2 t_2)]\,\mathrm{d}\omega_1\mathrm{d}\omega_2. \tag{17}$$

Again, we find the average temporal intensity by setting $t_1 = t_2 = t$,

$$I(t) = \Gamma(t,t) = \langle |E(t)|^2\rangle, \tag{18}$$

which is generally time dependent. The complex degree of temporal coherence is then

$$\gamma(t_1,t_2)=\frac{\Gamma(t_1,t_2)}{\sqrt{I(t_1)I(t_2)}}, \tag{19}$$

and it satisfies the inequalities

$$0\le|\gamma(t_1,t_2)|\le 1. \tag{20}$$

Finally, the overall degree of temporal coherence is

$$\bar{\gamma}=\sqrt{\frac{\int\int_0^\infty|\Gamma(t_1,t_2)|^2\mathrm{d}t_1\mathrm{d}t_2}{\int\int_0^\infty I(t_1)I(t_2)\mathrm{d}t_1\mathrm{d}t_2}}, \tag{21}$$

which is again limited to the interval [0, 1]. The overall degree of coherence also has the following property:

$$\bar{\gamma}=\bar{\mu}. \tag{22}$$

In other words, the overall degree of coherence must have the same value in both temporal and spectral domains. This follows directly from Eqs. (3) and (4), as well as the application of Parseval's theorem.

The correlation functions introduced here are so-called 'second-order' correlations, signifying the number of fields present in the definition. There is some ambiguity in the nomenclature, and in quantum photonics language these are "first-order" correlations, since they deal with fields and not intensities. Some authors prefer to make a distinction between the field and intensity correlations by instead calling any correlation function with n coordinates an "n-coordinate" correlation function. Then the above functions would be two-coordinate correlation functions of the first order (defined with fields, not intensities). These can be further generalized to higher orders and coordinate pairs, and we will be adopting this definition for the rest of the tutorial.

C. Stationary Light

So far, we have been talking about the more general form of the CSD and MCF, and the preceding forms apply for nonstationary light, such as pulses. However, none of the considerations above can be used to form a continuous field with a broad spectrum, such as black-body radiation. In order to construct such a model, we need to introduce *statistically stationary* light. A statistically stationary field contains random temporal fluctuations of amplitude, phase, and polarization. More importantly, the statistical properties of such a field are the same no matter when we choose to measure them, hence the word stationary. From this we already see that pulses can never be stationary, since one of their statistical properties, the average intensity, is time dependent.

The requirement of statistical stationarity is quite restrictive, since all statistical measures have to be independent of time, including correlation functions up to infinite coordinate pairs and orders. However, it is often enough to consider fields for which only the first two statistical measures (the average field and average intensity) are time independent. Fields that are called *wide-sense stationary* fulfill this requirement.

To find the stationary limit, we reverse Eq. (12), that is, find the CSD by multiplying the complex degree of coherence with the corresponding spectral densities

$$W(\omega_1,\omega_2)=\sqrt{S(\omega_1)S(\omega_2)}\mu(\omega_1,\omega_2). \tag{23}$$

Then we again rotate the coordinates by 45 deg to obtain

$$W(\omega,\Delta\omega)=\sqrt{S(\omega-\Delta\omega/2)S(\omega+\Delta\omega/2)}\mu(\omega,\Delta\omega), \tag{24}$$

after which we approximate that the spectral density is much wider than $\mu(\omega,\Delta\omega)$ along the $\Delta\omega$ direction, and that $\mu(\omega,\Delta\omega)$ is invariant along ω. This is the quasi-homogeneous approximation [35], which allows us to write

$$W(\omega,\Delta\omega)\approx S(\omega)\mu(\Delta\omega). \tag{25}$$

Inserting this into Eq. (17) and integrating over $\Delta\omega$, we arrive at

$$\Gamma(t,\Delta t)=\Omega_c A(t)\int_0^\infty S(\omega)\exp(-i\omega\Delta t)\,\mathrm{d}\omega, \tag{26}$$

where $\Delta t=t_2-t_1$ is the time difference, Ω_c is related to the spectral coherence width of the distribution chosen for $\mu(\Delta\omega)$, and $A(t)$ is a dimensionless envelope function. The stationary case is retrieved when the envelope becomes independent of time, i.e., $A(t)=A_0$. This happens in the limit $\Omega_c\to 0$, i.e., when spectral correlations vanish. Note that this also causes the MCF to tend toward zero.

To obtain a finite and nonzero correlation function for a stationary field, the energy spectrum $S(\omega)$ must contain an infinite amount of energy. This is consistent with the definition of stationarity, since the field must have a constant intensity over an infinite time interval. One can then rewrite the above integral as the Wiener–Khintchine theorem

$$\Gamma(\Delta t)=\int_0^\infty S^{(s)}(\omega)\exp(-i\omega\Delta t)\,\mathrm{d}\omega, \tag{27}$$

with $S^{(s)}(\omega)$ being the *power spectrum* of a statistically stationary field, which contains contributions from $\Omega_c\to 0$, $A(t)\to A_0$, and $S(\omega)\to\infty$. Note that although such a field must carry an infinite energy, the power spectrum itself is finite. A more physically relevant field is obtained when the constant intensity is chosen to last over a certain temporal window, which forces some of the frequencies to become partially correlated. If there are some spectral correlations, we often call such fields quasi-stationary.

The left-hand side of Eq. (27) defines a first-order, single coordinate correlation function, which is the MCF for stationary light. It is enough to completely characterize the temporal correlations of stationary light. Since we recover the average intensity by setting $t_1=t_2$, we immediately see that the average intensity, $\Gamma(0)=I$, is independent of time. In other words, light is stationary when there are no correlations between frequency components, i.e., a (wide sense) statistically stationary field is spectrally incoherent since $\Omega_c\to 0$. The only exceptions to this are perfectly monochromatic fields, for which it is meaningless to talk about spectral coherence.

Moreover, in the stationary limit the field usually becomes ergodic, meaning that the time and ensemble averages coincide. In other words, for stationary light it does not matter whether one uses the ensemble or time average, although it makes a large difference for nonstationary fields. Last, by Fourier inversion we see that

$$S^{(s)}(\omega) = \frac{1}{2\pi}\int_{-\infty}^{\infty} \Gamma(\Delta t)\exp(i\omega\Delta t)\,\mathrm{d}\Delta t. \quad (28)$$

Hence, $S^{(s)}(\omega)$ and $\Gamma(\Delta t)$ form a Fourier transform pair. Note that this applies also in the case of nonstationary light, although $\Gamma(\Delta t)$ contains only a part of the correlation information for a nonstationary field. We can measure $\Gamma(\Delta t)$ with a Michelson interferometer, and see a fringe visibility with varying Δt (path difference). This has immediate applications, such as optical coherence tomography [36,37] or Fourier transform spectroscopy [38].

4. PROPERTIES OF NONSTATIONARY FIELDS

Nonstationary fields have several properties that are not found in their stationary counterparts, while there are also some that are shared between the two. In the following subsections, we will look at the basic properties of nonstationary fields, with an emphasis on experimental aspects.

A. Pulse Length and Shape

For coherent fields, we usually write the time domain field as

$$E(t) = \sqrt{I(t)}\exp[i\phi(t) - i\omega_c t]\,, \quad (29)$$

where $\sqrt{I(t)}$ is the time-dependent (real valued) envelope, ω_c is the carrier frequency, and $\phi(t)$ is the temporal phase. In the spectral domain, the same field can be written as

$$\tilde{E}(\omega) = \sqrt{S(\omega)}\exp[i\varphi(\omega)]\,, \quad (30)$$

where $\sqrt{S(\omega)}$ is the frequency-dependent (real valued) envelope centered around ω_c, and $\varphi(\omega)$ is the spectral phase. A coherent pulse is at its shortest when it has a flat phase, i.e., when $\varphi(\omega)$ is constant. This is called a transform-limited pulse, since its length is limited only by the properties of Fourier transform. Due to the Fourier relation between time and space, a transform-limited pulse becomes shorter the wider its spectrum is. The length of the pulse can then be quantified with standard measures, such as full-width at half-maximum (FWHM), $1/e^2$ width, or root-mean-squared (rms) width.

When the pulse is partially coherent, the situation is a bit different. In this case, the spectral phase fluctuates from pulse to pulse around some well-defined mean value $\varphi_m(\omega)$, which can be separated from the random variable $\varphi_r(\omega)$, as in

$$\tilde{E}(\omega) = \sqrt{S(\omega)}\exp[i\varphi_m(\omega) + i\varphi_r(\omega)]\,. \quad (31)$$

Hence, even if one were to find a flat mean spectral phase, the random fluctuations will prevent the pulse from attaining the transform-limited form.

To quantify this, we need to turn back to the correlation functions. We can take the generalized Wiener–Khintchine theorem, and set $t_1 = t_2 = t$, to find the mean intensity

$$I(t) = \Gamma(t,t) = \int_{-\infty}^{\infty}\int_{0}^{\infty} W(\omega,\Delta\omega)\exp(-i\Delta\omega t)\,\mathrm{d}\omega\mathrm{d}\Delta\omega, \quad (32)$$

where we have again rotated the CSD by 45 deg. This shows that the whole CSD function contributes to the length of the pulse.

We can take this a step further, and integrate over the difference coordinate to get

$$I(t) = \int_{0}^{\infty} W_g(\omega,t)\mathrm{d}\omega, \quad (33)$$

where $W_g(\omega,t)$ is the Wigner function corresponding to the CSD. The intensity is then given by a marginal over the Wigner function, from where we see that if we want a constant intensity, then the Wigner function must be infinitely wide along the t direction. This further implies that the CSD must be infinitesimally narrow along the $\Delta\omega$ direction due to the Fourier relation between the rotated CSD and the Wigner function. Hence, we have confirmed our assumption of spectral incoherence of stationary fields.

To further illustrate the effect of coherence on pulse length, let us consider a specific example. Let us take again the case of a quasi-homogeneous field, for which the CSD is given by Eq. (25). Inserting this into Eq. (32), we get

$$I(t) = \int_{0}^{\infty} S(\omega)\mathrm{d}\omega\int_{-\infty}^{\infty}\mu(\Delta\omega)\exp(-i\Delta\omega t)\,\mathrm{d}\Delta\omega, \quad (34)$$

from which it is easy to see that the integral over ω yields the total intensity of the temporal pulse, whereas $\mu(\Delta\omega)$ dictates the pulse shape. Note that since $\mu(\Delta\omega)$ is a narrow function, its Fourier transform must therefore be wide compared to the transform-limited pulse. In the limit of $\mu(\Delta\omega)$ becoming infinitesimally narrow, we again arrive at the stationary case [31], as outlined in Section 3.C.

B. Propagation through Free Space

Propagation of pulsed beams can be carried out with the standard angular spectrum method (see, e.g. [25], p. 109 *et seq.*). For this purpose, we employ the Fourier transform relation between time and frequency of Eqs. (3) and (4), as well as between space and spatial frequency, as in

$$\tilde{A}(\boldsymbol{\kappa};\omega) = \frac{1}{(2\pi)^2}\iint_{-\infty}^{\infty}\tilde{E}(\boldsymbol{\rho},0;\omega)\exp(-i\boldsymbol{\kappa}\cdot\boldsymbol{\rho})\,\mathrm{d}^2\rho, \quad (35)$$

where $\boldsymbol{\rho} = (x,y)$, $\tilde{A}(\boldsymbol{\kappa};\omega)$ is the angular spectrum of the field, $\boldsymbol{\kappa} = (k_x,k_y)$ contains the transverse wave vector components, and we have started the propagation from an arbitrary plane denoted as $z = 0$. Note that the absolute value of the angular spectrum has no z dependence in linear propagation problems, and that in free space the refractive index is $n(\omega) = 1$. Propagation is then handled by multiplying the angular spectrum with a propagation phase, and inverse Fourier transforming, as in

$$\tilde{E}(\boldsymbol{\rho},z;\omega) = \iint_{-\infty}^{\infty}\tilde{A}(\boldsymbol{\kappa};\omega)\exp(ik_z z)\exp(i\boldsymbol{\kappa}\cdot\boldsymbol{\rho})\,\mathrm{d}^2\kappa, \quad (36)$$

where

$$k_z = \sqrt{k^2 - \kappa^2}, \quad (37)$$

where $\kappa = |\boldsymbol{\kappa}|$. This propagation method is relatively straightforward and, yet, quite general: any field that can be expressed as a superposition of plane waves can be propagated with it. While

the angular spectrum method is conceptually simple, there are only a handful of scenarios where it can be analytically carried out. In practice, it is usually done numerically.

In the case of beams, we can employ the paraxial approximation of k_z to make things simpler:

$$k_z \approx k - \frac{\kappa^2}{2k}, \tag{38}$$

which are the first two terms from the Taylor expansion of k_z. Substituting this into Eq. (36), and then using Eq. (35), we can integrate over $\boldsymbol{\kappa}$ and simplify to get

$$\tilde{E}(\boldsymbol{\rho},z;\omega) = \frac{k\exp(ikz)}{i2\pi z}\iint_{-\infty}^{\infty}\tilde{E}(\boldsymbol{\rho}',0;\omega) \times \exp\left[\frac{ik}{2z}\left(\boldsymbol{\rho}-\boldsymbol{\rho}'\right)^2\right]\mathrm{d}^2\rho', \tag{39}$$

which is the well-known Fresnel propagation formula. Here we denote the initial plane ($z=0$) transverse coordinates with a prime ($\boldsymbol{\rho}'$) to set them apart from the transverse coordinates ($\boldsymbol{\rho}$) at the plane of propagation ($z\neq 0$). From here, it is quite simple to further approximate far-zone propagation to get the Fraunhofer formula.

Propagation of partially coherent light follows the same principle as coherent light. We can use Eq. (36) in the definition of the CSD of Eq. (10), which we can rearrange into the form

$$W(\boldsymbol{\rho}_1,\boldsymbol{\rho}_2,z;\omega_1,\omega_2) = \iiiint_{-\infty}^{\infty} T(\boldsymbol{\kappa}_1,\boldsymbol{\kappa}_2;\omega_1,\omega_2) \times \exp\left[-i\left(k_{z1}^{*}-k_{z2}\right)z\right] \times \exp\left[-i\left(\boldsymbol{\kappa}_1\cdot\boldsymbol{\rho}_1-\boldsymbol{\kappa}_2\cdot\boldsymbol{\rho}_2\right)\right]\mathrm{d}^2\kappa_1\mathrm{d}^2\kappa_2, \tag{40}$$

from where we can identify the angular correlation function (ACF), as in

$$T(\boldsymbol{\kappa}_1,\boldsymbol{\kappa}_2;\omega_1,\omega_2) = \langle\tilde{A}^{*}(\boldsymbol{\kappa}_1;\omega_1)\tilde{A}(\boldsymbol{\kappa}_2;\omega_2)\rangle = \frac{1}{(2\pi)^4}\iiiint_{-\infty}^{\infty} W(\boldsymbol{\rho}_1,\boldsymbol{\rho}_2;\omega_1,\omega_2) \times \exp\left[i\left(\boldsymbol{\kappa}_1\cdot\boldsymbol{\rho}_1-\boldsymbol{\kappa}_2\cdot\boldsymbol{\rho}_2\right)\right]\mathrm{d}^2\rho_1\mathrm{d}^2\rho_2. \tag{41}$$

Note that in Eq. (40), we have chosen $z_1 = z_2 = z$, so that we are concerned with the correlation function at a specific plane of propagation. It is also possible to look at z coherence [39–41].

We can proceed as in the coherent case and consider the propagation of paraxial fields, such that the first two terms of the Taylor expansion

$$k_{zj} \approx k_j - \frac{\kappa_j^2}{2k_j} \tag{42}$$

are sufficient to model the propagation properties of such fields. Here $k_j = |\boldsymbol{k}_j| = \omega_j/c_0$ is the magnitude of the wave vector evaluated at the frequency ω_j, with $j\in(1,2)$, and similarly for κ_j. Using this approximation and inputting from Eq. (41) into Eq. (40) and integrating with respect to $\boldsymbol{\kappa}_1$ and $\boldsymbol{\kappa}_2$ yields the Fresnel propagation formula for partially coherent light:

$$W(\boldsymbol{\rho}_1,\boldsymbol{\rho}_2,z;\omega_1,\omega_2) = \frac{k_1k_2\exp(i\Delta kz)}{4\pi^2z^2}\iiiint_{-\infty}^{\infty} W(\boldsymbol{\rho}_1',\boldsymbol{\rho}_2';\omega_1,\omega_2) \times \exp\left[-ik\frac{c_1(\boldsymbol{\rho}_1-\boldsymbol{\rho}_1')^2-c_2(\boldsymbol{\rho}_2-\boldsymbol{\rho}_2')^2}{2z}\right]\mathrm{d}^2\boldsymbol{\rho}_1'\mathrm{d}^2\boldsymbol{\rho}_2', \tag{43}$$

where $\Delta k = k_2 - k_1$, and we have defined a spectral scaling factor $c_j = \omega_j/\omega_c$, with ω_c being some reference frequency, such as the carrier or center frequency of the field. In the present form, the equation can be used to propagate a nonstationary paraxial field to an arbitrary plane z. However, the quadruple integral is quite cumbersome to evaluate, and since it describes the field in the spatiospectral domain, it must also be transformed to the spatiotemporal domain to match experimental settings. It is possible to introduce approximations such as narrow bandwidth ($c_1\approx c_2\approx 1$, e.g., a few percent of center frequency) and/or far-zone propagation to cast the integrals into a more manageable form. Notably, it is possible to recast this as a topological problem, where propagation is governed by a continuous deformation of the corresponding Wigner function [42]. Note that the narrow bandwidth approximation cannot be employed for ultrashort pulses of several tens of femtoseconds in duration. There is no sharp limit where the approximation breaks down, but rather the breakdown is gradual.

C. Spatiotemporal Coupling

A common property of polychromatic fields is that they feature spatiotemporal coupling; i.e., the temporal properties of the field depend on the spatial position and vice-versa. In fact, this is a very general property. Let us say that we have a CSD that factors into space and frequency contributions at the initial plane, such that we can write

$$W(\boldsymbol{\rho}_1',\boldsymbol{\rho}_2';\omega_1,\omega_2) = W_s(\boldsymbol{\rho}_1',\boldsymbol{\rho}_2')\,W_f(\omega_1,\omega_2). \tag{44}$$

With this choice, we see that the spectral properties of the field do not depend on the spatial position, and therefore there is no spatiotemporal coupling either. If we input this into the propagation integral of Eq. (43), we get

$$W(\boldsymbol{\rho}_1,\boldsymbol{\rho}_2,z;\omega_1,\omega_2) = \frac{k_1k_2\exp(i\Delta kz)}{4\pi^2z^2}W_f(\omega_1,\omega_2)\iiiint_{-\infty}^{\infty} W_s(\boldsymbol{\rho}_1',\boldsymbol{\rho}_2') \times \exp\left[-ik\frac{c_1(\boldsymbol{\rho}_1-\boldsymbol{\rho}_1')^2-c_2(\boldsymbol{\rho}_2-\boldsymbol{\rho}_2')^2}{2z}\right]\mathrm{d}^2\boldsymbol{\rho}_1'\mathrm{d}^2\boldsymbol{\rho}_2', \tag{45}$$

from which we immediately see that different frequencies have very different spatial scaling due to the factors c_j. Strictly

speaking, this causes the field to immediately become spatiotemporally coupled upon propagation, if it has any spectral bandwidth at all.

However, in many cases the coupling is weak and can be neglected. For example, in spherical-mirror laser resonators the waist of the beam is frequency dependent [43], satisfying the relation

$$w(\omega) = \sqrt{\frac{\omega_c}{\omega}} w_0, \tag{46}$$

where w_0 is the beam waist at the reference frequency ω_c. This has the consequence that the Rayleigh range loses its frequency dependence

$$z_R = \frac{\omega}{2c_0} n w^2(\omega) = \frac{\omega_c}{2c_0} n w_0^2, \tag{47}$$

where $n = n(\omega) \sim$ constant within the bandwidth of the beam. This is the definition of an isodiffracting field, and it is by construction spatiotemporally coupled. To propagate it, one needs to find the supported modes of the cavity, propagate each of them individually, and then construct the correlation function from the propagated fields. This is a relatively straightforward procedure, but the analytical calculations can be very lengthy. Still, even in this case, the coupling becomes significant only for single- or sub-cycle pulses, i.e., pulses comparable to, or shorter than, a single optical cycle [44,45].

On the other hand, ultrashort pulses may feature strong spatiotemporal distortions after interaction with optical elements. Nonideal lenses that cause aberrations are a common source of coupling [46], and care must be taken when designing an optical experiment. Moreover, propagation through nonlinear media causes the spatial and temporal degrees of freedom to become linked in a nontrivial manner [47]. Some measures of spatiotemporal coupling have been introduced in the literature [46,48], although there is no single widely employed method for quantifying such coupling. One relatively simple technique is to take the spatiospectral phase, $\varphi(\boldsymbol{\rho};\omega)$ and expand it in a Taylor series around a point $\xi = (\boldsymbol{\rho};\omega)$. Then, the coefficients of the expansion are directly proportional to the strength of the coupling, being quite similar to the measures introduced in [48].

Of course, spatiotemporal coupling is not always detrimental. There are several field configurations that are designed to be spatiotemporal. These include skyrmions, hopfions, spatiotemporal optical vortices, orbital angular momentum carrying pulses, as well as spatiotemporal wave packets [49–58], to name a few. Each one of these features a specific type of coupling, which must be introduced with a carefully designed experimental setup. For an overview of the progress in designing, generating, and employing spatiotemporal light fields, see [59].

5. SPECTRAL EFFECTS

It is often taken for granted that the spectrum of light does not change on free-space propagation or when two beams of light are superposed. However, such assumptions may be violated by radiation emanating from nonconventional light sources such as pulsed lasers. This was made evident in Section 4.C, where we noted that the spatial and temporal degrees of freedom generally depend on each other. Conditions under which the normalized spectrum remains unchanged during these instances are specified by the notions of cross-spectral purity [60,61] and spectral invariance of light [62].

In this section, we give a brief outline of the two concepts in the context of nonstationary light propagating in vacuum ($n(\omega) = 1$). Moreover, we review a method of generating cross-spectrally pure and spectrally invariant fields from isodiffracting pulsed beams by spectral scale transformations using hybrid refractive–diffractive imaging systems.

A. Cross-Spectral Purity

Cross-spectral purity is characterized by two-beam interference of light where the normalized spectrum of the superposition is the same as that of the interfering fields [60,61]. The concept has been assessed in many situations dealing with partially coherent scalar light [63–67], and established also for electromagnetic fields in both stationary [68–70] and nonstationary domains [71,72]. Below, we present the concept for nonstationary scalar fields, where we summarize the results of [73,74].

Consider a superposition of two fields from positions $\mathbf{r}_1$ and $\mathbf{r}_2$ at some observation point $\mathbf{R}$. A single spectral realization of the superposition field at frequency ω is given by [74,75]

$$\begin{aligned}\tilde{E}(\mathbf{R};\omega) &= \tilde{E}(\mathbf{r}_1;\omega)\exp(i\omega t_1) + \tilde{E}(\mathbf{r}_2;\omega)\exp(i\omega t_2)\\ &= [\tilde{E}(\mathbf{r}_1;\omega) + \tilde{E}(\mathbf{r}_2;\omega)\exp(-i\omega\tau)]\exp(i\omega t_1),\end{aligned} \tag{48}$$

where $t_j = R_j/c_0$, R_j represents the path length from $\mathbf{r}_j$ to $\mathbf{R}$, $j \in (1,2)$, and $\tau = t_1 - t_2$. Superposition of this form can be implemented, e.g., in wavefront-shearing or -folding interferometers [75], and it excludes the typical frequency-dependent factors present in the traditional interferometric configurations, such as Young's two-pinhole experiment [25,75]. The requirement for cross-spectral purity of light at $\mathbf{r}_1$ and $\mathbf{r}_2$ is formulated as follows. If the normalized spectrum

$$s(\mathbf{r};\omega) = \frac{S(\mathbf{r};\omega)}{\int_0^\infty S(\mathbf{r};\omega)\mathrm{d}\omega} \tag{49}$$

is the same for the fields at $\mathbf{r}_1$ and $\mathbf{r}_2$ and for the superposition at $\mathbf{R}$ corresponding to some value $\tau = \tau_0$, i.e.,

$$s(\mathbf{r}_1;\omega) = s(\mathbf{r}_2;\omega) = s(\mathbf{R};\omega), \tag{50}$$

the fields at $\mathbf{r}_1$ and $\mathbf{r}_2$ are cross-spectrally pure. Generally, the condition above may be satisfied either everywhere in the domain of analysis or only at certain pairs of points. This leads to the following two categories [74]:

(i). If the normalized spectra at points $\mathbf{r}_1$ and $\mathbf{r}_2$ are the same and the delay τ_0 exists for these points, which fulfills the second equality above, the fields at $\mathbf{r}_1$ and $\mathbf{r}_2$ are *locally* cross-spectrally pure.

(ii). If the requirements in (i) are fulfilled for all possible pairs of points within some region—such as a cross-section of a light beam—the light in that region is *globally* cross-spectrally pure.

One might expect that cross-spectral purity is more common locally rather than globally, although there is no evidence to

prove that this is the case. At the very least, local purity is simple to facilitate experimentally, since any partially coherent beam can be transformed into a locally cross-spectrally pure beam with a specular CSD [76–78]. A CSD is called specular when it satisfies $W(\boldsymbol{\rho}_1,\boldsymbol{\rho}_2;\omega_1,\omega_2) = W(-\boldsymbol{\rho}_1,\boldsymbol{\rho}_2;\omega_1,\omega_2)$, in which case cross-spectral purity is satisfied at symmetric positions $\boldsymbol{\rho}_1$ and $\boldsymbol{\rho}_2 = -\boldsymbol{\rho}_1$ along the cross section of a beam. On the other hand, beams with a CSD of the separable form given by Eq. (44) are globally cross-spectrally pure across the plane on which the factorization holds. In other words, a globally cross-spectrally pure field is not spatiotemporally coupled at some specific plane of propagation. However, as noted above, purity vanishes and the field becomes coupled as it propagates any finite distance from that plane [73].

A specific property of cross-spectrally pure light fields is the reducibility of the coherence functions. For stationary light, this is manifested by the complex degree of temporal coherence satisfying the reduction formula [60,61]

$$\gamma(\mathbf{r}_1,\mathbf{r}_2;\Delta t) = \gamma(\mathbf{r}_1,\mathbf{r}_1;\tau_0)\gamma(\mathbf{r}_1,\mathbf{r}_1;\Delta t-\tau_0), \tag{51}$$

which implies that the space-time domain coherence functions of a cross-spectrally pure stationary field decompose into two factors. One of these factors contains the information of spatial coherence at points $\mathbf{r}_1$ and $\mathbf{r}_2$, and the other characterizes temporal coherence at one of the points.

In the case of nonstationary fields, we note that the MCF in Eq. (16) contains dependence on the two temporal coordinates instead of their difference Δt, implying that the space-time domain correlation functions of a nonstationary field cannot be applied directly to the expression above. However, an analogous result can be formulated in terms of the time-integrated MCF

$$\bar{\Gamma}(\mathbf{r}_1,\mathbf{r}_2,\,\Delta t) = \int_{-\infty}^{\infty}\Gamma(\mathbf{r}_1,\mathbf{r}_2;t,\Delta t)\mathrm{d}t \tag{52}$$

and the associated degree of coherence

$$\bar{\gamma}(\mathbf{r}_1,\mathbf{r}_2;\Delta t) = \frac{\bar{\Gamma}(\mathbf{r}_1,\mathbf{r}_2;\Delta t)}{\sqrt{\bar{\Gamma}(\mathbf{r}_1,\mathbf{r}_1;0)\bar{\Gamma}(\mathbf{r}_2;\mathbf{r}_2,0)}}, \tag{53}$$

with $t = (t_1+t_2)/2$. In particular, it can be shown that the reduction formula [74]

$$\bar{\gamma}(\mathbf{r}_1,\mathbf{r}_2;\Delta t) = \bar{\gamma}(\mathbf{r}_1,\mathbf{r}_2;\tau_0)\bar{\gamma}(\mathbf{r}_1,\mathbf{r}_1;\Delta t-\tau_0) \tag{54}$$

holds for cross-spectrally pure nonstationary fields. The degree of coherence associated with the time-integrated MCF thus factors into a product of spatial and temporal parts, which is similar to the stationary-field result in Eq. (51).

As a last remark of this subsection, we briefly comment on the measurement of cross-spectral purity. Since the wavefront folding and shearing interferometers can be used to form the superposition of Eq. (48), they can also be used to quantify cross-spectral purity. One just needs to measure the spectrum of the incident light from the two arms individually, as well as in the superposition (with, e.g., a fiber spectrometer).

B. Spectral Invariance

The concept of spectral invariance, introduced by Wolf in 1986, refers to a situation where the normalized spectrum in the far zone of a planar, secondary source is invariant with respect to the far-field observation direction, and equal to the normalized source spectrum [62]. In particular, the celebrated Wolf's scaling law specifies the condition for the spatial coherence of a quasi-homogeneous light source [25] under which light emanating from a source is spectrally invariant. The scaling law is satisfied in many common situations, although light sources that violate it can be easily found and designed. In the latter case, remarkable spectral effects such as red- and blue-shifting may take place [79–84]. Spectral invariance has been extensively studied in the context of stationary light [85–90], and very recently extended to nonstationary fields [91].

Spectral invariance is an enabling factor in astronomy, since Wolf showed that usual interstellar objects radiate light that satisfies the scaling law. Moreover, it has added significance in nonstationary optics, since an invariant spectrum implies that the temporal domain properties may also be conserved upon propagation to the far zone. In what follows, we review the concept of spectral invariance for nonstationary light and present the nonstationary-field version of the scaling law.

The spectrum of a field in the far zone of a planar, secondary light source is obtained by employing the angular spectrum representation of Eq. (36) together with the method of stationary phase (see [25], p. 128 *et seq.*), and is given by

$$S^{(\infty)}(\hat{\boldsymbol{s}};\omega) = \left(\frac{2\pi s_z}{r}\right)^2\left(\frac{\omega}{c_0}\right)^2 T\left(\frac{\omega}{c_0}\boldsymbol{\sigma},\frac{\omega}{c_0}\boldsymbol{\sigma};\omega,\omega\right). \tag{55}$$

Here $\hat{\boldsymbol{s}} = (\boldsymbol{\sigma},s_z)$ is a unit vector that specifies the observation direction in the far zone, with $\boldsymbol{\sigma} = (s_x,s_y)$ and s_z representing the transverse and longitudinal components of $\hat{\boldsymbol{s}}$, r being the distance from the source, and $T(\boldsymbol{\kappa}_1,\boldsymbol{\kappa}_2;\omega_1,\omega_2)$ being the angular correlation function from Eq. (41). Further, the normalized spectrum in the far zone is written as

$$s^{(\infty)}(\hat{\boldsymbol{s}};\omega) = \frac{S^{(\infty)}(\hat{\boldsymbol{s}};\omega)}{\int_0^\infty S^{(\infty)}(\hat{\boldsymbol{s}};\omega)\mathrm{d}\omega}. \tag{56}$$

We define the condition for a nonstationary light field to be spectrally invariant as follows. First, the normalized far-zone spectrum is required to be independent of observation direction, $s^{(\infty)}(\hat{\boldsymbol{s}};\omega) = s^{(\infty)}(\omega)$. Second, the normalized spectrum at the far zone must be equal to the normalized source-integrated spectrum

$$\bar{s}(\omega) = \frac{\bar{S}(\omega)}{\int_0^\infty \bar{S}(\omega)\mathrm{d}\omega}, \tag{57}$$

with $\bar{S}(\omega) = \int_0^\infty S(\boldsymbol{\rho};\omega)\mathrm{d}^2\rho$ being the source-integrated spectral density. We remark that the second requirement is a relaxed version of that in [62] for stationary fields, where the spectrum is demanded to be constant across the source plane. Such a generalization is physically appropriate, since the spectrum in many natural and manmade light sources exhibits spatial variations across the source plane.

It was shown in [91] that the conditions $s^{(\infty)}(\hat{\boldsymbol{s}},\omega) = s^{(\infty)}(\omega) = \bar{s}(\omega)$ are satisfied for a source whose CSD is of the form

$$W(\boldsymbol{\rho}_1,\boldsymbol{\rho}_2;\omega_1,\omega_2) = [S(\boldsymbol{\rho};\omega_1)S(\boldsymbol{\rho};\omega_2)]^{1/2}g(\boldsymbol{\rho}_1,\boldsymbol{\rho}_2;\omega_1,\omega_2), \tag{58}$$

with $\boldsymbol{\rho} = (\boldsymbol{\rho}_1 + \boldsymbol{\rho}_2)/2$, and the function $g(\boldsymbol{\rho}_1, \boldsymbol{\rho}_2; \omega_1, \omega_2)$ obeying

$$g(\boldsymbol{\rho}_1, \boldsymbol{\rho}_2; \omega, \omega) = \nu(\Delta\boldsymbol{\rho}; \omega) = \frac{H(\omega \Delta\boldsymbol{\rho}/c_0)}{H(0)}, \tag{59}$$

where $\Delta\boldsymbol{\rho} = \boldsymbol{\rho}_2 - \boldsymbol{\rho}_1$. Above, $H(\omega\Delta\boldsymbol{\rho}/c_0)$ is a function containing dependence on the spatial and spectral variables solely via the product $\omega\Delta\boldsymbol{\rho}$. The expression in Eq. (59) forms the scaling law for spectral invariance of nonstationary fields, which ensures that the normalized spectrum of light is the same across the far zone and equal to the normalized source-integrated spectrum. In addition, we remark that the form above reduces to Wolf's scaling law when stationary and quasi-homogeneous fields are considered. In particular, if the single-frequency CSD of a stationary field is of the form $W(\boldsymbol{\rho}_1, \boldsymbol{\rho}_2; \omega) = S(\omega)\nu(\Delta\boldsymbol{\rho}; \omega)$, the function $\nu(\Delta\boldsymbol{\rho}; \omega)$ must obey the latter equality in Eq. (59) for the field to be spectrally invariant.

Furthermore, for quasi-homogeneous sources mentioned in Section 4.A, we have $\nu(\Delta\boldsymbol{\rho}; \omega) \approx \mu(\Delta\boldsymbol{\rho}; \omega)$. This leads to the original Wolf's scaling law, which states that the information on the degree of coherence at all frequencies is obtained from the degree of coherence at a single frequency by scaling the position difference $\Delta\boldsymbol{\rho}$.

C. Experimental Aspects

Next, we present a feasible method for transforming isodiffracting pulsed beams into nonstationary fields exhibiting either cross-spectral purity or spectral invariance, as described in [92]. Isodiffracting beams, as outlined in Section 4.C, are specified by their frequency-independent Rayleigh range, which is caused by the spectral scaling of the beam waist given by Eq. (46). Such fields are generated in paraxial spherical-mirror laser resonators, forming an important class of model fields in nonstationary optics. Such beams are thus an appealing starting point for the transformations.

We begin by considering the CSD of an isodiffracting field at frequencies ω_1 and ω_2, which is given by [45]

$$\begin{aligned} W(\boldsymbol{\rho}_1, \boldsymbol{\rho}_2; \omega_1, \omega_2) = &\left(\frac{\omega_1}{\omega_c}\frac{\omega_2}{\omega_c}\right)^{1/2} [S_0(\omega_1) S_0(\omega_2)]^{1/2} \\ &\times \exp\left(-\frac{1+\beta^2}{2\beta}\frac{\omega_1 \boldsymbol{\rho}_1^2 + \omega_2 \boldsymbol{\rho}_2^2}{\omega_c w_0^2}\right) \\ &\times \exp\left(\frac{1-\beta^2}{\beta}\frac{\sqrt{\omega_1\omega_2}}{\omega_c}\frac{\boldsymbol{\rho}_1 \cdot \boldsymbol{\rho}_2}{w_0^2}\right). \end{aligned} \tag{60}$$

Above, $S_0(\omega)$ is a spectral weight function, and $0 \le \beta \le 1$, where $\beta = 1$ corresponds to complete spatial coherence of the field, $\beta \ll 1$ implies that the field is quasi-homogeneous, and $\beta \to 0$ corresponds to spatial incoherence.

To accomplish the transformations, we employ paraxial afocal imaging systems. Such systems add a chromatic compensation to the isodiffracting beam, modifying the spectral scaling of the beam waist so that the beam at the system output is of the desired form in each transformation. In the design process, the paraxial $ABCD$ system matrix is used, which, for an afocal imaging system, has the expression [93]

$$\mathbf{M}(\omega) = \begin{bmatrix} A(\omega) & B(\omega) \\ C(\omega) & D(\omega) \end{bmatrix} = \begin{bmatrix} M(\omega) & 0 \\ 0 & 1/M(\omega) \end{bmatrix}. \tag{61}$$

Here $M(\omega)$ represents the frequency-dependent magnification of the system. The effect of the system on the input field can be assessed by employing the Collins diffraction integral [94] and using the method of stationary phase at the limit $B(\omega) \to 0$. As shown in [92], the resulting CSD at the output plane of a system illuminated by an input isodiffracting beam is

$$\begin{aligned} &W(\boldsymbol{\rho}_1, \boldsymbol{\rho}_2; \omega_1, \omega_2) \\ &= \frac{\exp(i\Delta\omega L/c_0)}{M(\omega_1)M(\omega_2)}\left(\frac{\omega_1}{\omega_c}\frac{\omega_2}{\omega_c}\right)^{1/2} [S_0(\omega_1) S_0(\omega_2)]^{1/2} \\ &\quad \times \exp\left\{-\frac{1+\beta^2}{2\beta}\left[\frac{\omega_1}{\omega_c}\frac{\boldsymbol{\rho}_1^2}{M^2(\omega_1)w_0^2} + \frac{\omega_2}{\omega_c}\frac{\boldsymbol{\rho}_2^2}{M^2(\omega_2)w_0^2}\right]\right\} \\ &\quad \times \exp\left[\frac{1-\beta^2}{\beta}\frac{\sqrt{\omega_1\omega_2}}{\omega_c}\frac{\boldsymbol{\rho}_1 \cdot \boldsymbol{\rho}_2}{M(\omega_1)M(\omega_2)w_0^2}\right], \end{aligned} \tag{62}$$

where L represents the axial length of the system. From the expression above, one can see that with a proper choice of the magnification, $M(\omega)$, the coherence properties of the input beam may be tailored to meet the requirements of the desired transformations.

For a cross-spectrally pure output field, we aim to produce a CSD of the separable form given by Eq. (44), which implies lack of space-frequency coupling and thus cross-spectral purity of the beam at the system output plane. In particular, we find that the choice

$$M(\omega) = \sqrt{\frac{\omega}{\omega_c}} M(\omega_c) \tag{63}$$

leads to a separable CSD, with the space and frequency factors being

$$\begin{aligned} W_s(\boldsymbol{\rho}_1, \boldsymbol{\rho}_2) = &\frac{1}{M(\omega_c)} \exp\left[-\frac{1+\beta^2}{2\beta}\frac{\boldsymbol{\rho}_1^2 + \boldsymbol{\rho}_2^2}{M^2(\omega_c)w_0^2}\right] \\ &\times \exp\left[\frac{1-\beta^2}{\beta}\frac{\boldsymbol{\rho}_1 \cdot \boldsymbol{\rho}_2}{M^2(\omega_c)w_0^2}\right] \end{aligned} \tag{64}$$

and

$$W_f(\omega_1, \omega_2) = \exp(i\Delta\omega L/c_0)[S_0(\omega_1) S_0(\omega_2)]^{1/2}, \tag{65}$$

respectively. Note that the magnitude of the magnification in Eq. (64) can be chosen arbitrarily, while preserving the spectral characteristics of Eq. (65). In other words, this type of system offers ideal, distortion-free focusing of isodiffracting pulsed beams.

On the other hand, when pursuing a spectrally invariant output field, we select

$$M(\omega) = \sqrt{\frac{\omega_c}{\omega}} M(\omega_c). \tag{66}$$

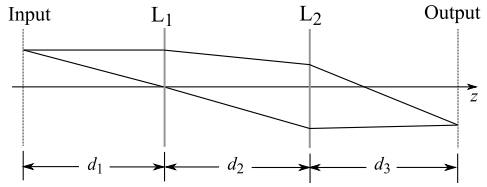

Fig. 1. Lens system geometry for the spectral scale transformations. Lenses L_1 and L_2 are (refractive or diffractive) thin lenses at positions defined by distances d_1, d_2, and d_3 between the system input and output planes.

This leads to the output CSD being expressible as in Eq. (58), where the factor $g(\boldsymbol{\rho}_1,\boldsymbol{\rho}_2;\omega_1,\omega_2)$ satisfies the scaling law of Eq. (59):

$$g(\boldsymbol{\rho}_1,\boldsymbol{\rho}_2;\omega,\omega) = v(\Delta\boldsymbol{\rho};\omega) = \exp\left[-\left(\frac{\omega}{\omega_c}\right)^2 \frac{\Delta\boldsymbol{\rho}^2}{2M^2(\omega_c)w^2\beta^2}\right]. \quad \textbf{(67)}$$

This ensures that no matter what the spectrum is, its shape will be preserved upon far-zone propagation, and that the spectrum is invariant with respect to the observation direction. This further implies that the temporal profile of the field is the same across the whole wavefront if the field does not meet any dispersive material during propagation.

In [92] it was shown that systems with magnifications given by Eqs. (63) and (66) can be approximately realized with hybrid designs whose geometry is illustrated in Fig. 1. Both designs consist of one refractive achromatic lens and one diffractive lens [95]. The focal lengths of the lenses are the same for both systems, while the order of the lenses and their separations from the conjugate planes specify the nature of the transformation. For cross-spectrally pure output, the diffractive lens is positioned before the achromat in Fig. 1, and the separations d_j, $j \in (1, 2, 3)$, are chosen so that the magnification

$$M(\omega) = \frac{3\omega - \omega_c}{2\omega} M(\omega_c) \quad \textbf{(68)}$$

is achieved (see [92] for details). The form above coincides with the ideal magnification of Eq. (63) at $\omega = \omega_c$ and approximates it otherwise, with the accuracy of the approximation illustrated in Fig. 2(a). Further, reversing the arrangement leads to a magnification

$$M(\omega) = \frac{\omega + \omega_c}{2\omega} M(\omega_c), \quad \textbf{(69)}$$

which is, in turn, an approximation of Eq. (66). The accuracy of this approximation is demonstrated in Fig. 2(b).

Next, we evaluate the precision of the two systems in accomplishing the desired transformations, where we choose a model weight function $S_0(\omega)$ of the power-exponential form [45,96]

$$[S_0(\omega)]^{1/4} = \left(\frac{\omega_c}{\omega}\right)^{1/4} \frac{1}{\sqrt{\Gamma(2p)}} \left(2p\frac{\omega}{\omega_c}\right)^p \exp\left(-p\frac{\omega}{\omega_c}\right). \quad \textbf{(70)}$$

Above, ω_c is the center frequency, p is a real positive constant that can be varied to control the spectral bandwidth, and $\Gamma(x)$ is the gamma function. We have chosen $p = 5$, which corresponds to an ultra-broadband isodiffracting beam [45].

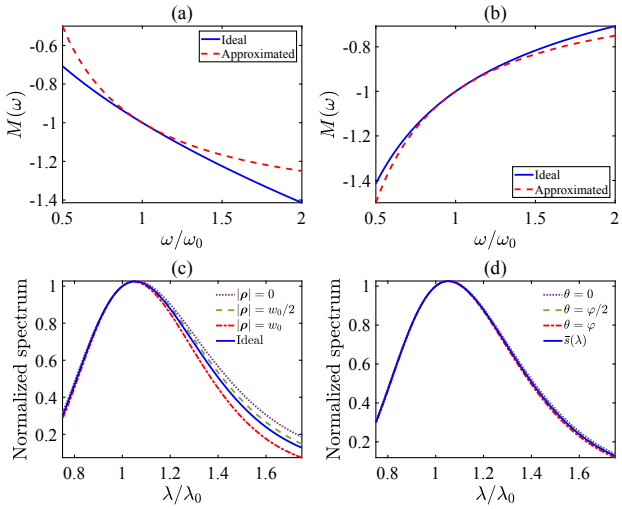

Fig. 2. First row: comparison between the ideal and approximated magnifications $M(\omega)$ for (a) cross-spectral purity and (b) spectral invariance at output of the transformation system, with $M(\omega_c) = -1$. Second row: (c) normalized spectrum at the spatial positions $|\boldsymbol{\rho}| = 0$, $|\boldsymbol{\rho}| = w_0/2$, and $|\boldsymbol{\rho}| = w_0$ at the output plane of the system with the approximated magnification of Eq. (68), plotted over a range of wavelengths λ around the wavelength $\lambda_c = 2\pi c_0/\omega_c$. In addition, the normalized spectrum of an ideal cross-spectrally pure field obtained with the magnification of Eq. (63) is shown. (d) Normalized source-integrated spectrum at the output plane of the system with the magnification of Eq. (69), and the normalized far-field spectra at directions $\theta = 0$, $\theta = \phi/2$, and $\theta = \phi$ proportional to the $1/e^2$ divergence angle ϕ. The spectra in (c) and (d) are normalized by the values at $\lambda = \lambda_c$. Adapted from [92].

In Fig. 2(c), we have plotted the normalized spectra obtained by substituting the approximate magnification of Eq. (68) into Eq. (49) and using Eq. (49). Further, we have chosen $\beta = 0.1$ and $M(\omega_c) = -1$. The normalized spectra at three radial positions across the transversal beam width are depicted at the output plane of the system designed to generate a cross-spectrally pure beam. The graph also includes the ideal normalized spectrum obtained by using Eqs. (44), (49), (64), and (65). The transformation yields a nearly cross-spectrally pure field in the proximity of the wavelength $\lambda_c = 2\pi c_0/\omega_c$ and maintains a reasonable level of accuracy when $\lambda/\lambda_c < 1$. However, departure from the ideal becomes more pronounced at longer wavelengths. To be specific, the normalized spectrum widens relative to the ideal along points on the optical axis and gradually narrows with increasing radial distance from the axis.

Figure 2(d) demonstrates the performance of the system aimed at producing a spectrally invariant output field. The figure displays the normalized far-field spectra obtained by employing Eqs. (62) and (69) together with Eqs. (41), (55), and (56), at three specific observation directions. In addition, the figure includes the normalized spatially averaged source spectrum for the secondary source at the system's output plane, calculated by placing the magnification from Eq. (69) into Eq. (62) and using Eq. (57). We note that the curves depicted in Fig. 2(d) are essentially indistinguishable when $\lambda < \lambda_c$, and they maintain a relatively close correspondence at long wavelengths. The on-axis

far-field spectrum exhibits a slight increase in width compared to the source-averaged spectrum, narrowing as the observation angle increases. Comparing Figs. 2(c) and 2(d), it is evident that the approximative magnification in Eq. (69) is more accurate at generating a spectrally invariant field than the magnification in Eq. (68) is at producing a cross-spectrally pure field.

6. MEASUREMENT SCHEMES

Measurement of nonstationary fields is one of the major technological challenges in photonics. In the present tutorial we will focus on the measurement of visible light, with limited applicability to infrared and ultraviolet regions. For information on plausible measurement schemes in these wavelength regions, see [97–99]. While the spatial properties of nonstationary fields can be characterized with time-averaging methods (see [75] for a review of spatial coherence measurement techniques), the temporal/spectral properties require more attention. This is inherently due to the time-dependent nature of the fields, and methods such as Michelson interferometry do not capture the essential details of nonstationary fields [100]. Several pulse measurement techniques have been introduced over the years [32,46,48,101,102], and here we give a very brief overview on some of the most common techniques that can be used to detect partial temporal coherence.

A. Frequency-Resolved Optical Gating

One of the first setups to measure pulse shapes was the intensity autocorrelation (see, e.g., [102] p. 66 *et seq.*). The method is very simple: take a linearly polarized pulse, split it into two, rotate the polarization of one of the copies by 90 deg, and overlap them at a second harmonic generating crystal as a function of time delay. The resulting second harmonic signal is then proportional to the original pulse. However, the problem with this method is that the retrieval of the original pulse from such a signal does not have a unique solution. That is, one signal can correspond to more than one pulse. This problem becomes more pronounced if the repetition rate of the laser is so high that single-shot measurements cannot be carried out.

Frequency-resolved optical gating (FROG) resolves this ambiguity by introducing spectral resolution to the detection. The resulting FROG interferogram for a single pulse is essentially unique [103], and the original pulse can be unambiguously recovered with an iterative retrieval algorithm (when there is no measurement error). The method outlined above is the fundamental FROG instrumentation, now known as the second harmonic generating (SHG) FROG, which is depicted in Fig. 3(a). There is a large family of different types of FROG measurement setups, such as polarization gating FROG, spatial encoded arrangement for temporal analysis by dispersing a pair of light E-fields (SEA-TADPOLE), as well as spatially and temporally resolved intensity and phase evaluation device: full information from a single hologram (STRIPED FISH).

However, all of the multishot FROG instruments share their fundamental properties, and as such we will limit our discussion to the SHG FROG. Introducing spectral resolution allows one to increase the available information on the pulse to iteratively retrieve its amplitude and phase. The interferogram one

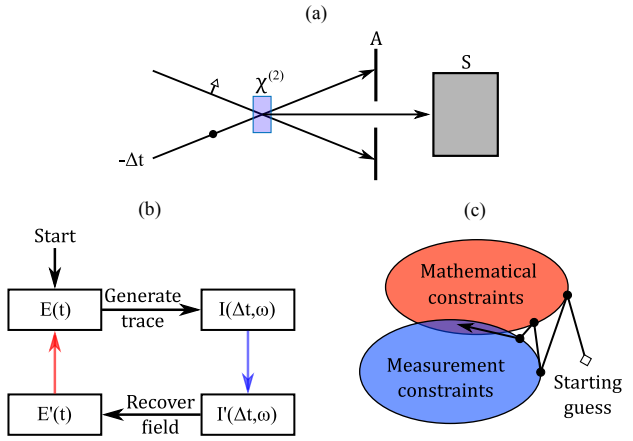

Fig. 3. (a) Fundamental components for an SHG FROG: two copies of a pulse with orthogonal polarizations are mixed in a second harmonic generating crystal with varying delay Δt. A is aperture, and S is an imaging spectrometer. (b) Flowchart of FROG retrieval algorithm, color coded to correspond to the application of the constraints in (c). The correct solution is somewhere within the overlapping constraints in (c), and the space of solutions that satisfy both constraints becomes bigger with decreasing coherence, and increasing measurement error.

measures from an SHG FROG obeys the equation

$$I_{\mathrm{SHG}}(\Delta t,\omega)=\left|\int_{-\infty}^{\infty}E(t)E(t-\Delta t)\exp(-i\omega t)\mathrm{d}t\right|^2. \quad (71)$$

It is notable that the interferogram is superficially similar to the Wigner distribution,

$$W_g(t,\omega)=\int_{-\infty}^{\infty}E^*(t)E(t-\Delta t)\exp(-i\omega\Delta t)\mathrm{d}\Delta t, \quad (72)$$

although there is no clear connection between the two. One of the well-known properties of the Wigner distribution is that its marginals yield expectation values; that is, integration over time gives the mean energy spectrum and integration over frequency the average temporal pulse. Because of this similarity, one may be tempted to look at the marginals of the FROG interferogram to find these properties. Unfortunately, only the energy spectrum can be retrieved from the marginals [104], and we are forced to use iterative methods if we wish to also find the temporal pulse shape.

A FROG retrieval algorithm generally works as outlined in the flowchart of Fig. 3(b): start from a guess for the pulse length and spectrum, and mathematically construct an interferogram. Then, discard the amplitude of the resulting FROG trace and replace it with the experimentally measured one, while retaining the phase. Finally, invert the interferogram to find how the pulse and spectrum have changed and update your guess. In essence, what this algorithm retrieves is not the pulse, but the phase of the interferogram, which can be used to find the pulse. The convergence of this algorithm is a key issue, and for pulses with sufficiently low complexity (small time–bandwidth product), it is fairly reliable. Figure 3(c) depicts the convergence properties of the algorithm with a Venn diagram, showing that there are essentially two constraints that need to be fulfilled.

When the pulse train is completely coherent, FROG can reliably find the pulse shape and phase. However, for partially coherent light, the situation is slightly different. The interferogram of a single pulse still follows Eq. (71), but since each pulse in the train is generally speaking different, the resulting interferogram also varies from pulse to pulse. If the detector is slow compared to the repetition rate of the pulse train, then the resulting time-averaged interferogram is an incoherent sum of the individual interferograms. The time-averaged version does not correspond to any single pulse, and therefore the retrieval is no longer unique. The algorithm can only estimate a typical pulse belonging to the sum, and the so-called FROG error will be high.

To properly assess the coherence properties of a partially coherent pulse train with FROG, one will need single-shot capabilities to measure a large number of individual pulses from the train. Afterwards, it is possible to numerically construct the correlation function describing the pulse train [105]. However, this method does not capture the effect of carrier-envelope offset phase (unless the pulse is on the order of a single cycle) and linear spectral phase. These properties must be measured with alternative methods, such as f-to-2f interferometry [106] and time-of-arrival measurements with an oscilloscope and a fast detector, respectively.

FROG devices with single-shot modes include STRIPED FISH, and grating-eliminated no-nonsense observation of ultrafast incident laser light E-fields (GRENOUILLE). If the repetition rate of the pulse train is very high (megahertz to gigahertz), then single-shot measurements may not be feasible. In such situation one is forced to make a rough evaluation of the coherence properties numerically [107].

B. Spectral Phase Interferometry for Direct Electric Field Reconstruction

Whenever two signals with different carrier frequencies are superposed, the result will be a time-dependent interference pattern, such as the one in Eq. (7). In principle, it is possible to find the phase difference between the two interfering waves. However, it is nearly impossible in practice, due to the extremely high frequency of visible light. To date, there are no methods that directly measure signals at sufficiently high sampling frequencies to directly evaluate phase differences between optical fields of appreciable bandwidth. Spectral interferometry (SI) circumvents this problem by using a reference pulse, which must be known, stable, and contain the same frequency components as the pulse to-be-measured (i.e., they must spectrally overlap).

SI is a linear method that can be used to find the signal pulse without iterative retrieval methods. However, the requirement of a known and stable reference pulse at the desired frequency is experimentally very demanding. Spectral phase interferometry for direct electric field reconstruction (SPIDER) is a self-referencing technique, which is not quite as demanding [32,101]. But similarly to most FROG techniques, this method also requires a nonlinearity.

The concept behind SPIDER is shown in Fig. 4: two pulses separated by a time delay τ are sum-frequency mixed with an orthogonally polarized and massively chirped pulse. The spectral interference pattern is then recorded with a spectrometer.

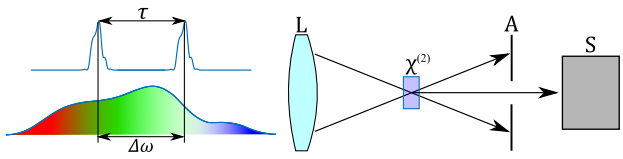

Fig. 4. Basic configuration for a SPIDER apparatus. A pulse pair is inserted into a second-order nonlinear crystal together with an orthogonally polarized and massively chirped pulse, where all three pulses are derived from the same initial pulse. The nonlinear crystal is cut for sum-frequency generation, and the upconverted pulse pair is selected with the aperture A and measured with the spectrometer S.

The chirped pulse is used to accomplish a spectral shear, since the frequencies in the pulse separate temporally when the chirp is large enough, and the temporal separation τ determines the fringe spacing in the resulting spectral interference pattern.

Obviously, this is just one variation of SPIDER, though it may be the most common one. Any device that mixes a pulse with a spectral slice of itself in a sum-frequency generating crystal, and then measures the spectral interference between two upconverted pulses, can be considered to be in the same family of experimental methods. SPIDER is often considered to be a temporal domain measurement, since the end goal is to find the shape of the temporal pulse. But it is in fact more appropriate to consider it as a frequency domain method, since it measures the spectral interference pattern at the detector, which is given by

$$S(\omega,\Delta\omega)=\left\langle\left|E_{\mathrm{u}}(\omega-\Delta\omega/2)+E_{\mathrm{u}}(\omega+\Delta\omega/2)\exp(-i\omega\tau)\right|^2\right\rangle, \tag{73}$$

where the subscript u denotes the upconverted pulse obtained via sum-frequency generation. Following the conventions in the earlier sections, we can write the spectral fringe pattern in the form

$$\begin{aligned}S(\omega,\Delta\omega)&=S_{\mathrm{u}}(\omega-\Delta\omega/2)+S_{\mathrm{u}}(\omega+\Delta\omega/2)\\&\quad+2\sqrt{S_{\mathrm{u}}(\omega-\Delta\omega/2)S_{\mathrm{u}}(\omega+\Delta\omega/2)}\\&\quad\times\Re\left\{\mu_{\mathrm{u}}(\omega,\Delta\omega)\exp(-i\omega\tau)\right\},\end{aligned} \tag{74}$$

from which we see that the SPIDER apparatus measures a slice from the spectral correlation function μ_u along the ω direction at a fixed spectral shear $\Delta\omega$.

Note that this correlation function corresponds to the upconverted pulse. One slice is enough to directly find the spectral phase of a coherent original pulse [108–110], as long as the spectral shear is sufficiently larger than zero. If $\Delta\omega=0$, then the phase terms exactly cancel out, and the measurement yields only the spectral density. Even at a moderate spectral shear, the high frequency phase components wash out for partially coherent pulses, and the method yields an erroneous result for the pulse length [111]. If one is able to measure the correlation function of the upconverted pulse train for all combinations of spectral coordinates (ω, $\Delta\omega$), and relate the upconverted field to the original field, then SPIDER can be used to measure the whole correlation function of the original pulse train [112]. Unfortunately, such a method has not been experimentally demonstrated as of yet.

C. Field Cross-Correlation

There are cases where one can obtain a realistic pulse length estimate, but the spectral phases of individual pulses cannot be measured with standard techniques, due to limitations caused by high repetition rate, incompatible wavelength region, or low incident power. In such cases, a linear self-referencing method, such as the field cross correlation [113], is desirable to probe the stability of the field.

Let us say that we have a pulse train from where we pick two different pulses and interfere them. This can be done with, e.g., an unbalanced Michelson interferometer, if the repetition rate is high enough [114]. In this case, the temporal field is given by

$$E(\boldsymbol{\rho};t,\Delta t) = E_i(\boldsymbol{\rho};t) + E_j(\boldsymbol{\rho};t+\Delta t), \tag{75}$$

where i,j correspond to different pulses, and the time delay Δt can be chosen such that they overlap between the pulses varies. If this superposition is directed to a slow detector, it will measure the time-averaged intensity pattern, which is of the form

$$I(\boldsymbol{\rho};\Delta t) = I_i(\boldsymbol{\rho}) + I_j(\boldsymbol{\rho}) + 2\Re\left\{\int \langle E_i^*(\boldsymbol{\rho};t)E_j(\boldsymbol{\rho};t+\Delta t)\rangle \mathrm{d}t\right\}, \tag{76}$$

where I_i and I_j stand for the individual time-integrated pulse intensities, and angle brackets denote ensemble averaging over a large number of pulses. The last part of this relation is the cross-correlation term, $\langle X(\boldsymbol{\rho};\Delta t)\rangle = \int \langle E_i^*(\boldsymbol{\rho};t)E_j(\boldsymbol{\rho};t+\Delta t)\rangle \mathrm{d}t$, and therefore we can write

$$I(\boldsymbol{\rho};\Delta t) = I_i(\boldsymbol{\rho}) + I_j(\boldsymbol{\rho}) + 2|\langle X(\boldsymbol{\rho};\Delta t)\rangle| \cos[\Phi(\boldsymbol{\rho};\Delta t)], \tag{77}$$

where $\Phi(\boldsymbol{\rho};\Delta t)$ is the phase of the cross correlation. The absolute value of the cross-correlation term is encoded into the visibility of interference fringes, while the phase is found from their positions.

In [113], it was found that it is possible to approximate

$$\langle X(\boldsymbol{\rho};0)\rangle \approx \bar{\mu}(\boldsymbol{\rho})\sqrt{I_i(\boldsymbol{\rho})I_j(\boldsymbol{\rho})}, \tag{78}$$

which can be substituted directly into Eq. (77) together with the choice $\Delta t = 0$, to obtain

$$I(\boldsymbol{\rho};0) \approx I_i(\boldsymbol{\rho}) + I_j(\boldsymbol{\rho}) + 2\sqrt{I_i(\boldsymbol{\rho})I_j(\boldsymbol{\rho})}|\bar{\mu}(\boldsymbol{\rho})| \cos[\Phi(\boldsymbol{\rho},0)], \tag{79}$$

Therefore, the overall spectral degree of coherence—which is a useful measure of the stability of the field—can be evaluated with only one temporal measurement point, which happens to be at zero time delay. Moreover, the approximation of Eq. (78) becomes better the more coherent the measured field is.

Measuring the cross-correlation trace across the full breadth of delays where it is visible also allows one to approximate the detailed spectral coherence properties, since

$$S_{\mathrm{qc}}(\boldsymbol{\rho};\omega) = \mathcal{F}^{-1}\{|\langle X(\boldsymbol{\rho};\Delta t)\rangle| \cos[\Phi(\boldsymbol{\rho};\Delta t)]\} = \mathcal{F}^{-1}\{[I(\boldsymbol{\rho};\Delta t) - I_i(\boldsymbol{\rho}) - I_j(\boldsymbol{\rho})]/2\}, \tag{80}$$

where $\mathcal{F}^{-1}$ denotes the inverse Fourier transform, and $S_{\mathrm{qc}}(\boldsymbol{\rho};\omega)$ is the quasi-coherent part of the spectrum [115,116]. Comparing this with the overall energy spectrum $S(\boldsymbol{\rho};\omega)$ allows one to find the portions of the spectral field that feature high or low coherence [113].

7. DISCUSSION AND CONCLUSIONS

The present tutorial covers the essentials of nonstationary optics, starting from the basic building blocks and fundamental objects of study—that is, monochromatic plane waves and correlation functions, respectively—and going through some of the main properties, as well as the associated measurement schemes. The tutorial includes the definitions of nonstationary coherence in time and frequency, as well as a brief discussion about the stationary limit. Properties such as pulse length and shape, propagation through free space, and spatiotemporal coupling were considered in detail. In all cases, the whole correlation function contributes to the problem, which underlines the importance of including statistical fluctuations through the CSD and MCF, when necessary.

Special attention to spectral effects was warranted, since cross-spectral purity and spectral invariance are fundamental properties of light, although they are generally not fulfilled. Notably, the device for introducing desired spectral scaling transformations allows one to achieve ideal focusing without spatiotemporal coupling. Finally, some of the most popular pulse measurement schemes—FROG and SPIDER—were discussed from the coherence theoretic point of view. In particular, the connection between increased FROG error and partial temporal/spectral coherence was explicitly stated. Moreover, the capability of SPIDER in measuring spectral correlations of the upconverted pulse was pointed out.

However, only the bare essentials were covered in the present work. The tutorial does not discuss the generation and manipulation of nonstationary waves, apart from a superficial level. Additionally, many topics were excluded, such as the connection between coherence and polarization [117–123], time-dependent polarization modulation [124–127], geometric phase [127–132], correlation-induced effects [42,85,133–138], and interaction between nonstationary fields and matter [139–143], just to name a few.

Nonstationary optics is an active and vibrant area of research, with several possible research directions. These include the research of fundamental aspects, such as the study of structured light fields, the polarization and coherence of three dimensional light, as well as correlation-induced effects. Moreover, nonstationary optics hosts a wide range of application oriented research areas, such as micromachining, pulse generation, and the measurement of nonstationary fields. In particular, the generation and measurement have been historically important, since shorter pulses have allowed greater advances in multiple related areas. Overall, nonstationary optics is expected to provide a large number of important advances in the near future.

Funding. Research Council of Finland (333938, 346518); Joensuu University Foundation.

Acknowledgment. JL acknowledges support from the Joensuu University Foundation.

Disclosures. The authors declare no conflicts of interest.

Data availability. No data were generated or analyzed in the presented research.

REFERENCES

1. J. W. Yoon, Y. G. Kim, I. W. Choi, *et al.*, "Realization of laser intensity over 10^{23} W/cm^2," Optica **8**, 630–635 (2021).
2. X. Liu, D. Du, and G. Mourou, "Laser ablation and micromachining with ultrashort laser pulses," IEEE J. Quantum Electron. **33**, 1706–1716 (1997).
3. C. B. Schaffer, A. Brodeur, J. F. García, *et al.*, "Micromachining bulk glass by use of femtosecond laser pulses with nanojoule energy," Opt. Lett. **26**, 93–95 (2001).
4. G. D. Valle, R. Osellame, and P. Laporta, "Micromachining of photonic devices by femtosecond laser pulses," J. Opt. A: Pure Appl. Opt. **11**, 013001 (2008).
5. A. Zewail, "Laser femtochemistry," Science **242**, 1645–1653 (1988).
6. A. Zewail, "Femtochemistry: atomic-scale dynamics of the chemical bond," J. Phys. Chem. A **104**, 5660–5694 (2000).
7. A. Zewail, "Femtochemistry. past, present, and future," Pure Appl. Chem. **72**, 2219–2231 (2000).
8. T. Udem, J. Reichert, R. Holzwarth, *et al.*, "Accurate measurement of large optical frequency differences with a mode-locked laser," Opt. Lett. **24**, 881–883 (1999).
9. T. Udem, J. Reichert, R. Holzwarth, *et al.*, "Absolute optical frequency measurement of the cesium d_1 line with a mode-locked laser," Phys. Rev. Lett. **82**, 3568–3571 (1999).
10. T. Udem, R. Holzwarth, and T. W. Hänsch, "Optical frequency metrology," Nature **416**, 233–237 (2002).
11. J. Klaers, J. Schmitt, F. Vewinger, *et al.*, "Bose–Einstein condensation of photons in an optical microcavity," Nature **468**, 545–548 (2010).
12. T. K. Hakala, A. J. Moilanen, A. I. Väkeväinen, *et al.*, "Bose-Einstein condensation in a plasmonic lattice," Nat. Phys. **14**, 739–744 (2018).
13. M. Maiuri, M. Garavelli, and G. Cerullo, "Ultrafast spectroscopy: state of the art and open challenges," J. Am. Chem. Soc. **142**, 3–15 (2020).
14. P. B. Corkum and Z. Chang, "The attosecond revolution," Opt. Photonics News **19**(10), 24–29 (2008).
15. F. Krausz, "The birth of attosecond physics and its coming of age," Phys. Scr. **91**, 063011 (2016).
16. X. F. Li, A. L'Huillier, M. Ferray, *et al.*, "Multiple-harmonic generation in rare gases at high laser intensity," Phys. Rev. A **39**, 5751–5761 (1989).
17. P. Antoine, A. L'Huillier, and M. Lewenstein, "Attosecond pulse trains using high–order harmonics," Phys. Rev. Lett. **77**, 1234–1237 (1996).
18. T. Gaumnitz, A. Jain, Y. Pertot, *et al.*, "Streaking of 43-attosecond soft-x-ray pulses generated by a passively CEP-stable mid-infrared driver," Opt. Express **25**, 27506–27518 (2017).
19. E. Goulielmakis, M. Uiberacker, R. Kienberger, *et al.*, "Direct measurement of light waves," Science **305**, 1267–1269 (2004).
20. E. Goulielmakis, Z.-H. Loh, A. Wirth, *et al.*, "Real-time observation of valence electron motion," Nature **466**, 739–743 (2010).
21. F. Calegari, D. Ayuso, A. Trabattoni, *et al.*, "Ultrafast electron dynamics in phenylalanine initiated by attosecond pulses," Science **346**, 336–339 (2014).
22. F. Calegari and F. Martin, "Open questions in attochemistry," Commun. Chem. **6**, 184 (2023).
23. A. Kaldun, A. Blättermann, V. Stooß, *et al.*, "Observing the ultrafast buildup of a Fano resonance in the time domain," Science **354**, 738–741 (2016).
24. V. Gruson, L. Barreau, A. Jiménez-Galan, *et al.*, "Attosecond dynamics through a Fano resonance: monitoring the birth of a photoelectron," Science **354**, 734–738 (2016).
25. L. Mandel and E. Wolf, *Optical Coherence and Quantum Optics* (Cambridge University, 1995).
26. M. Bertolotti, L. Sereda, and A. Ferrari, "Application of the spectral representation of stochastic processes to the study of nonstationary light radiation: a tutorial," Pure Appl. Opt. **6**, 153–171 (1997).
27. F. Zernike, "The concept of degree of coherence and its application to optical problems," Physica **5**, 785–795 (1938).
28. S. A. Ponomarenko, G. P. Agrawal, and E. Wolf, "Energy spectrum of a nonstationary ensemble of pulses," Opt. Lett. **29**, 394–396 (2004).
29. M. Bertolotti, A. Ferrari, and L. Sereda, "Coherence properties of nonstationary polychromatic light sources," J. Opt. Soc. Am. B **12**, 341–347 (1995).
30. L. Sereda, M. Bertolotti, and A. Ferrari, "Coherence properties of nonstationary light wave fields," J. Opt. Soc. Am. A **15**, 695–705 (1998).
31. P. Pääkkönen, J. Turunen, P. Vahimaa, *et al.*, "Partially coherent Gaussian pulses," Opt. Commun. **204**, 53–58 (2002).
32. I. A. Walmsley and C. Dorrer, "Characterization of ultrashort electromagnetic pulses," Adv. Opt. Photonics **1**, 308–437 (2009).
33. J. H. Eberly and K. Wódkiewicz, "The time-dependent physical spectrum of light," J. Opt. Soc. Am. **67**, 1252–1261 (1977).
34. M. Al lakki, A. T. Friberg, and T. Setälä, "Complete coherence of random, nonstationary electromagnetic fields," Opt. Lett. **46**, 1756–1759 (2021).
35. W. H. Carter and E. Wolf, "Coherence and radiometry with quasihomogeneous planar sources," J. Opt. Soc. Am. **67**, 785–796 (1977).
36. D. Huang, E. A. Swanson, C. P. Lin, *et al.*, "Optical coherence tomography," Science **254**, 1178–1181 (1991).
37. B. E. Bouma, J. F. de Boer, D. Huang, *et al.*, "Optical coherence tomography," Nat. Rev. Methods Primers **2**, 79 (2022).
38. J. Mandon, G. Guelachvili, and N. Picqué, "Fourier transform spectroscopy with a laser frequency comb," Nat. Photonics **3**, 99–102 (2009).
39. F. Gori, R. Martínez-Herrero, G. Piquero, *et al.*, "On z-coherence in self-focusing," Opt. Lett. **47**, 1681–1684 (2022).
40. M. Santarsiero, G. Piquero, J. C. G. de Sande, *et al.*, "On *z*-coherence of beams radiated by Schell-model sources with Gaussian profile," Opt. Lett. **47**, 2258–2261 (2022).
41. H. Chang, X. Cai, F. Wang, *et al.*, "On z-coherence of Schell-model sources carrying a prescribed astigmatic phase," Opt. Lett. **48**, 558–561 (2023).
42. M. Luo, M. Ornigotti, and M. Koivurova, "Inverse design of optical correlation induced effects," APL Photonics **8**, 086106 (2023).
43. S. Feng, H. G. Winful, and R. W. Hellwarth, "Spatiotemporal evolution of focused single-cycle electromagnetic pulses," Phys. Rev. E **59**, 4630–4649 (1999).
44. S. Feng and H. G. Winful, "Spatiotemporal structure of isodiffracting ultrashort electromagnetic pulses," Phys. Rev. E **61**, 862–873 (2000).
45. M. Koivurova, C. Ding, J. Turunen, *et al.*, "Partially coherent isodiffracting pulsed beams," Phys. Rev. A **97**, 023825 (2018).
46. S. Akturk, X. Gu, P. Bowlan, *et al.*, "Spatio-temporal couplings in ultrashort laser pulses," J. Opt. **12**, 093001 (2010).
47. A. Halder, V. Jukna, M. Koivurova, *et al.*, "Coherence of bulk-generated supercontinuum," Photonics Res. **7**, 1345–1353 (2019).
48. S. W. Jolly, O. Gobert, and F. Quéré, "Spatio-temporal characterization of ultrashort laser beams: a tutorial," J. Opt. **22**, 103501 (2020).
49. Y. Shen, Y. Hou, N. Papasimakis, *et al.*, "Supertoroidal light pulses as electromagnetic skyrmions propagating in free space," Nat. Commun. **12**, 5891 (2021).
50. Y. Shen, E. C. Martínez, and C. Rosales-Guzmán, "Generation of optical skyrmions with tunable topological textures," ACS Photonics **9**, 296–303 (2022).
51. C. Wan, Y. Shen, A. Chong, *et al.*, "Scalar optical hopfions," eLight **2**, 22 (2022).
52. N. Jhajj, I. Larkin, E. W. Rosenthal, *et al.*, "Spatiotemporal optical vortices," Phys. Rev. X **6**, 031037 (2016).
53. M. Ornigotti, C. Conti, and A. Szameit, "Effect of orbital angular momentum on nondiffracting ultrashort optical pulses," Phys. Rev. Lett. **115**, 100401 (2015).
54. M. A. Porras, "Upper bound to the orbital angular momentum carried by an ultrashort pulse," Phys. Rev. Lett. **122**, 123904 (2019).
55. M. A. Porras and R. Garca-Álvarez, "General laws of the propagation of few-cycle optical pulses with orbital angular momentum in free space," Phys. Rev. A **102**, 033522 (2020).

56. L. Ma, C. Chen, Z. Zhan, *et al.*, "Generation of spatiotemporal optical vortices in ultrashort laser pulses using rotationally interleaved multispirals," Opt. Express **30**, 47287–47303 (2022).
57. H. E. Kondakci and A. F. Abouraddy, "Optical space-time wave packets having arbitrary group velocities in free space," Nat. Commun. **10**, 929 (2019).
58. M. Yessenov, L. A. Hall, K. L. Schepler, *et al.*, "Space-time wave packets," Adv. Opt. Photonics **14**, 455–570 (2022).
59. Y. Shen, Q. Zhan, L. G. Wright, *et al.*, "Roadmap on spatiotemporal light fields," J. Opt. **25**, 093001 (2023).
60. L. Mandel, "Concept of cross-spectral purity in coherence theory," J. Opt. Soc. Am. **51**, 1342–1350 (1961).
61. L. Mandel and E. Wolf, "Spectral coherence and the concept of cross-spectral purity," J. Opt. Soc. Am. **66**, 529–535 (1976).
62. E. Wolf, "Invariance of the spectrum of light on propagation," Phys. Rev. Lett. **56**, 1370–1372 (1986).
63. D. F. James and E. Wolf, "Cross-spectrally pure light and the spectral modulation law," Opt. Commun. **138**, 257–261 (1997).
64. H. Kandpal, "Generation of cross-spectrally pure light by two diffusers moving in opposite directions and determination of diffuser surface roughness," Opt. Commun. **207**, 73–76 (2002).
65. H. Liu, J. Cheng, and S. Han, "Cross spectral purity and its influence on ghost imaging experiments," Opt. Commun. **273**, 50–53 (2007).
66. M. Lahiri and E. Wolf, "Statistical similarity and cross-spectral purity of stationary stochastic fields," Opt. Lett. **37**, 963–965 (2012).
67. M. Lahiri and E. Wolf, "Effect of scattering on cross-spectral purity of light," Opt. Commun. **330**, 165–168 (2014).
68. T. Hassinen, J. Tervo, and A. T. Friberg, "Cross-spectral purity of electromagnetic fields," Opt. Lett. **34**, 3866–3868 (2009).
69. T. Hassinen, J. Tervo, and A. T. Friberg, "Cross-spectral purity of the Stokes parameters," Appl. Phys. B **105**, 305–308 (2011).
70. T. Hassinen, J. Tervo, and A. T. Friberg, "Purity of partial polarization in the frequency and time domains," Opt. Lett. **38**, 1221–1223 (2013).
71. R. Joshi and B. Kanseri, "Cross-spectral purity of nonstationary vector fields in space–time and space–frequency domains," J. Opt. Soc. Am. A **38**, 271–276 (2021).
72. J. Laatikainen, A. T. Friberg, and T. Setälä, "Cross-spectral purity of the Stokes parameters in random nonstationary electromagnetic beams," Opt. Lett. **48**, 5823–5826 (2023).
73. M. Koivurova, C. Ding, J. Turunen, *et al.*, "Cross-spectral purity of nonstationary light," Phys. Rev. A **99**, 043842 (2019).
74. J. Laatikainen, M. Luo, A. Halder, *et al.*, "Reduction formula for cross-spectral purity of nonstationary light fields," J. Opt. Soc. Am. A **40**, 1260–1267 (2023).
75. J. Turunen, A. Halder, M. Koivurova, *et al.*, "Measurement of spatial coherence of light Invited," J. Opt. Soc. Am. A **39**, C214–C239 (2022).
76. F. Gori, G. Guattari, C. Palma, *et al.*, "Specular cross-spectral density functions," Opt. Commun. **68**, 239–243 (1988).
77. H. Partanen, N. Sharmin, J. Tervo, *et al.*, "Specular and antispecular light beams," Opt. Express **23**, 28718–28727 (2015).
78. D. Das, A. Halder, H. Partanen, *et al.*, "Propagation of Bessel-correlated specular and antispecular beams," Opt. Express **30**, 5709–5721 (2022).
79. E. Wolf, "Non-cosmological redshifts of spectral lines," Nature **326**, 363–365 (1987).
80. E. Wolf, "Red shifts and blue shifts of spectral lines emitted by two correlated sources," Phys. Rev. Lett. **58**, 2646–2648 (1987).
81. M. F. Bocko, D. H. Douglass, and R. S. Knox, "Observation of frequency shifts of spectral lines due to source correlations," Phys. Rev. Lett. **58**, 2649–2651 (1987).
82. G. M. Morris and D. Faklis, "Effects of source correlation on the spectrum of light," Opt. Commun. **62**, 5–11 (1987).
83. D. Faklis and G. M. Morris, "Spectral shifts produced by source correlations," Opt. Lett. **13**, 4–6 (1988).
84. F. Gori, G. Guattari, C. Palma, *et al.*, "Observation of optical redshifts and blueshifts produced by source correlations," Opt. Commun. **67**, 1–4 (1988).
85. E. Wolf and D. F. V. James, "Correlation-induced spectral changes," Rep. Prog. Phys. **59**, 771–828 (1996).
86. F. Gori, G. Marcopoli, and M. Santarsiero, "Spectrum invariance on paraxial propagation," Opt. Commun. **81**, 123–130 (1991).
87. H. Roychowdhury and E. Wolf, "Spectral invariance in fields generated by quasi-homogeneous scaling law sources," Opt. Commun. **215**, 199–203 (2003).
88. J. Pu, O. Korotkova, and E. Wolf, "Polarization-induced spectral changes on propagation of stochastic electromagnetic beams," Phys. Rev. E **75**, 056610 (2007).
89. O. Korotkova, J. Pu, and E. Wolf, "Spectral changes in electromagnetic stochastic beams propagating through turbulent atmosphere," J. Mod. Opt. **55**, 1199–1208 (2008).
90. B. Kanseri and H. C. Kandpal, "Experimental observation of invariance of spectral degree of coherence with change in bandwidth of light," Opt. Lett. **35**, 70–72 (2010).
91. C. Ding, M. Koivurova, T. Setälä, *et al.*, "Spectral invariance and scaling law for nonstationary optical fields," Phys. Rev. A **101**, 033808 (2020).
92. J. Laatikainen, M. Koivurova, J. Turunen, *et al.*, "Spectral scale transformations of nonstationary optical fields," Phys. Rev. A **106**, 023515 (2022).
93. J. W. Goodman, *Introduction to Fourier Optics*, 3rd ed. (Roberts & Company, 2005).
94. S. A. Collins, "Lens-system diffraction integral written in terms of matrix optics," J. Opt. Soc. Am. **60**, 1168–1177 (1970).
95. H. P. Herzig, "Design of refractive and diffractive micro-optics," in *Micro-optics: Systems, Components, and Applications*, H. P. Herzig, ed. (Taylor & Francis, 1997), pp. 1–29.
96. K. Saastamoinen, J. Turunen, P. Vahimaa, *et al.*, "Spectrally partially coherent propagation-invariant fields," Phys. Rev. A **80**, 053804 (2009).
97. R. A. Kaindl, M. Wurm, K. Reimann, *et al.*, "Generation, shaping, and characterization of intense femtosecond pulses tunable from 3 to 20 μm," J. Opt. Soc. Am. B **17**, 2086–2094 (2000).
98. P. K. Bates, O. Chalus, and J. Biegert, "Ultrashort pulse characterization in the mid-infrared," Opt. Lett. **35**, 1377–1379 (2010).
99. I. Orfanos, I. Makos, I. Liontos, *et al.*, "Attosecond pulse metrology," APL Photonics **4**, 080901 (2019).
100. M. Koivurova, L. Ahad, G. Geloni, *et al.*, "Interferometry and coherence of nonstationary light," Opt. Lett. **44**, 522–525 (2019).
101. C. Iaconis and I. A. Walmsley, "Spectral phase interferometry for direct electric-field reconstruction of ultrashort optical pulses," Opt. Lett. **23**, 792–794 (1998).
102. R. Trebino, *Frequency-Resolved Optical Gating: The Measurement of Ultrashort Laser Pulses* (Kluwer Academic, 2000).
103. L. Xu, E. Zeek, and R. Trebino, "Simulations of frequency-resolved optical gating for measuring very complex pulses," J. Opt. Soc. Am. B **25**, A70–A80 (2008).
104. R. Jafari, T. Jones, and R. Trebino, "100% reliable algorithm for second-harmonic-generation frequency-resolved optical gating," Opt. Express **27**, 2112–2124 (2019).
105. R. Talukder, A. Halder, M. Koivurova, *et al.*, "Generation of pulse trains with nonconventional temporal correlation properties," J. Opt. **24**, 055502 (2022).
106. D. J. Jones, S. A. Diddams, J. K. Ranka, *et al.*, "Carrier-envelope phase control of femtosecond mode-locked lasers and direct optical frequency synthesis," Science **288**, 635–639 (2000).
107. C. Bourassin-Bouchet and M.-E. Couprie, "Partially coherent ultrafast spectrography," Nat. Commun. **6**, 6465 (2015).
108. G. Stibenz and G. Steinmeyer, "High dynamic range characterization of ultrabroadband white-light continuum pulses," Opt. Express **12**, 6319–6325 (2004).
109. J. Wemans, G. Figueira, N. Lopes, *et al.*, "Self-referencing spectral phase interferometry for direct electric-field reconstruction with chirped pulses," Opt. Lett. **31**, 2217–2219 (2006).
110. J. Bethge, C. Grebing, and G. Steinmeyer, "A fast Gabor wavelet transform for high-precision phase retrieval in spectral interferometry," Opt. Express **15**, 14313–14321 (2007).
111. J. Ratner, G. Steinmeyer, T. C. Wong, *et al.*, "Coherent artifact in modern pulse measurements," Opt. Lett. **37**, 2874–2876 (2012).
112. B. J. Davis, "Observable coherence theory for statistically periodic fields," Phys. Rev. A **76**, 043843 (2007).

113. D. Show, A. Halder, T. K. Hakala, *et al.*, "Single-shot measurement of overall degree of spectral coherence: bulk-generated supercontinuum case," Phys. Rev. B **105**, 104310 (2022).
114. M. Närhi, J. Turunen, A. T. Friberg, *et al.*, "Experimental measurement of the second-order coherence of supercontinuum," Phys. Rev. Lett. **116**, 243901 (2016).
115. G. Genty, M. Surakka, J. Turunen, *et al.*, "Second-order coherence of supercontinuum light," Opt. Lett. **35**, 3057–3059 (2010).
116. M. Koivurova, "Randomness, determinism, and ignorance in coherence," Opt. Lett. **48**, 3187–3190 (2023).
117. O. Korotkova and E. Wolf, "Generalized Stokes parameters of random electromagnetic beams," Opt. Lett. **30**, 198–200 (2005).
118. T. Setälä, J. Tervo, and A. T. Friberg, "Stokes parameters and polarization contrasts in Young's interference experiment," Opt. Lett. **31**, 2208–2210 (2006).
119. E. Wolf, *Introduction to the Theory of Coherence and Polarization of Light* (Cambridge University, 2007).
120. J. Tervo, T. Setälä, A. Roueff, *et al.*, "Two-point Stokes parameters: interpretation and properties," Opt. Lett. **34**, 3074–3076 (2009).
121. T. Hassinen, J. Tervo, T. Setälä, *et al.*, "Hanbury Brown–Twiss effect with electromagnetic waves," Opt. Express **19**, 15188–15195 (2011).
122. A. T. Friberg and T. Setälä, "Electromagnetic theory of optical coherence Invited," J. Opt. Soc. Am. A **33**, 2431–2442 (2016).
123. J. Xu, G. Gbur, and T. D. Visser, "Generalization of Malus' law and spatial coherence relations for linear polarizers and non-uniform polarizers," Opt. Lett. **47**, 5739–5742 (2022).
124. T. Brixner and G. Gerber, "Femtosecond polarization pulse shaping," Opt. Lett. **26**, 557–559 (2001).
125. R. Selle, P. Nuernberger, F. Langhojer, *et al.*, "Generation of polarization-shaped ultraviolet femtosecond pulses," Opt. Lett. **33**, 803–805 (2008).
126. K. Misawa, "Applications of polarization-shaped femtosecond laser pulses," Adv. Phys.: X **1**, 544–569 (2016).
127. E. Pillinen, M. Koivurova, and J. Turunen, "Pulse shaping by spectral-domain polarization gratings," Opt. Lett. **47**, 2012–2015 (2022).
128. Z. Bomzon, G. Biener, V. Kleiner, *et al.*, "Space-variant Pancharatnam–Berry phase optical elements with computer-generated subwavelength gratings," Opt. Lett. **27**, 1141–1143 (2002).
129. A. Hannonen, K. Saastamoinen, L.-P. Leppänen, *et al.*, "Geometric phase in beating of light waves," New J. Phys. **21**, 083030 (2019).
130. A. Hannonen, H. Partanen, A. Leinonen, *et al.*, "Measurement of the Pancharatnam–Berry phase in two-beam interference," Optica **7**, 1435–1439 (2020).
131. A. Leinonen, A. Hannonen, H. Partanen, *et al.*, "Noncyclic continuous Pancharatnam—Berry phase in dual-beam interference," Commun. Phys. **6**, 132 (2023).
132. L. Garza-Soto, N. Hagen, D. Lopez-Mago, *et al.*, "Wave description of geometric phase," J. Opt. Soc. Am. A **40**, 388–396 (2023).
133. E. Wolf, "Correlation-induced changes in the degree of polarization, the degree of coherence, and the spectrum of random electromagnetic beams on propagation," Opt. Lett. **28**, 1078–1080 (2003).
134. R. W. Schoonover, B. J. Davis, and P. S. Carney, "The generalized wolf shift for cyclostationary fields," Opt. Express **17**, 4705–4711 (2009).
135. H. Lajunen and T. Saastamoinen, "Propagation characteristics of partially coherent beams with spatially varying correlations," Opt. Lett. **36**, 4104–4106 (2011).
136. S. Sahin and O. Korotkova, "Light sources generating far fields with tunable flat profiles," Opt. Lett. **37**, 2970–2972 (2012).
137. Y. Chen, J. Gu, F. Wang, *et al.*, "Self-splitting properties of a Hermite-Gaussian correlated Schell-model beam," Phys. Rev. A **91**, 013823 (2015).
138. C. Ding, M. Koivurova, J. Turunen, *et al.*, "Temporal self-splitting of optical pulses," Phys. Rev. A **97**, 053838 (2018).
139. P. Gibbon, *Short Pulse Laser Interactions with Matter: An Introduction* (Imperial College, 2005).
140. J.-C. Diels and W. Rudolph, *Ultrashort Laser Pulse Phenomena* (Academic, 2006).
141. G. A. Mourou, C. L. Labaune, M. Dunne, *et al.*, "Relativistic laser-matter interaction: from attosecond pulse generation to fast ignition," Plasma Phys. Controlled Fusion **49**, B667 (2007).
142. P. Forn-Daz, L. Lamata, E. Rico, *et al.*, "Ultrastrong coupling regimes of light-matter interaction," Rev. Mod. Phys. **91**, 025005 (2019).
143. N. Rivera and I. Kaminer, "Light–matter interactions with photonic quasiparticles," Nat. Rev. Phys. **2**, 538–561 (2020).